Biosensors and Bioelectronics 176 (2021) 112947

Contents lists available at ScienceDirect

Biosensors and Bioelectronics

journal homepage: http://www.elsevier.com/locate/bios

Aptamer-functionalized metal-organic frameworks (MOFs) for biosensing

Mengzhen Lv [a,b,1], Wan Zhou [b,1], Hamed Tavakoli [b,1], Cynthia Bautista [b], Jianfei Xia [a,b,**], Zonghua Wang [a], XiuJun Li [b,c,d,*]

[a] College of Chemistry and Chemical Engineering, Shandong Sino-Japanese Center for Collaborative Research of Carbon Nanomaterials, Qingdao University, Qingdao, 266071, PR China

[b] Department of Chemistry and Biochemistry, University of Texas at El Paso, El Paso, 79968, USA

[c] Biomedical Engineering, Border Biomedical Research Center, University of Texas at El Paso, El Paso, 79968, USA

[d] Environmental Science and Engineering, University of Texas at El Paso, El Paso, 79968, USA

ARTICLE INFO

Keywords:
Aptamer
Metal-organic frameworks (MOFs)
Stimuli-responsive
Microfluidic
Biosensor
Aptasensor

ABSTRACT

As a class of crystalline porous materials, metal-organic frameworks (MOFs) have attracted increasing attention. Due to the nanoscale framework structure, adjustable pore size, large specific surface area, and good chemical stability, MOFs have been applied widely in many fields such as biosensors, biomedicine, electrocatalysis, energy storage and conversions. Especially when they are combined with aptamer functionalization, MOFs can be utilized to construct high-performance biosensors for numerous applications ranging from medical diagnostics and food safety inspection, to environmental surveillance. Herein, this article reviews recent innovations of aptamer-functionalized MOFs-based biosensors and their bio-applications. We first briefly introduce different functionalization methods of MOFs with aptamers, which provide a foundation for the construction of MOFs-based aptasensors. Then, we comprehensively summarize different types of MOFs-based aptasensors and their applications, in which MOFs serve as either signal probes or signal probe carriers for optical, electrochemical, and photoelectrochemical detection, with an emphasis on the former. Given recent substantial research interests in stimuli-responsive materials and the microfluidic lab-on-a-chip technology, we also present the stimuli-responsive aptamer-functionalized MOFs for sensing, followed by a brief overview on the integration of MOFs on microfluidic devices. Current limitations and prospective trends of MOFs-based biosensors are discussed at the end.

1. Introduction

Metal-organic frameworks (MOFs), a type of crystalline nanomaterials composed of metal ions and organic ligands, were first defined in 1995 as porous coordination polymers (PCPs) (Yaghi et al., 1995; Zhu and Xu, 2014). Since then, numerous organic linkers have been developed to combine with various inorganic sites, leading to the formation of tens of thousands of MOFs with different compositions (Drake et al., 2018). Because of their large specific areas, facile synthesis approaches, abundant functional groups, and chemical stability (Li et al., 2018; Zhu et al., 2019), MOFs are widely utilized in various fields such as separation (Altintas et al., 2018), gas adsorption (Pham et al., 2017), energy storage (Wang et al., 2017a) and catalysis (Chughtai et al., 2015). Importantly, the following advantages of MOFs make them good candidates for the fabrication of biosensors with wide applications, especially in biomedical and environmental fields (Li et al., 2019; Liu et al., 2020). First, large specific areas and porous structures of MOFs provide more interfaces and active sites for interaction between materials and analytes. Second, the organic ligands with rich functional groups provide MOFs ease of functionalization with various molecules and materials, including nucleic acids, enzymes, nanoparticles, and so on. Finally, the diverse compositions of MOFs between metal and organic ligands offer a lot of functionality, such as catalytic activity, electrochemical activity, and optical activity; therefore, MOFs can be used as signal probes for different detection methods.

Aptamers were first reported in the early 1990s, and subsequently aroused much attention from researchers as an alternative to antibodies because they are more flexible, cost-effective, and stable (Espiritu et al.,

* Corresponding author. Department of Chemistry and Biochemistry, University of Texas at El Paso, El Paso, 79968, USA.
** Corresponding author. Department of Chemistry and Biochemistry, University of Texas at El Paso, El Paso, 79968, USA.
E-mail addresses: xiajianfei@126.com (J. Xia), xli4@utep.edu (X. Li).
[1] Denotes equal contributions.

https://doi.org/10.1016/j.bios.2020.112947
Received 31 May 2020; Received in revised form 22 December 2020; Accepted 26 December 2020
Available online 30 December 2020

2018). Aptamers are new classes of oligonucleotides (or peptides) belonging to "functional nucleic acids" with many remarkable merits, including simple synthesis, a wide variety of specific targets, excellent stability, and non-immunogenicity (Kholafazad Kordasht et al., 2020). Aptamers usually have a length of approximate 25–80 bases with high affinity and specificity (Ni et al., 2020), and can distinguish a wide variety of molecules such as organic dyes, bacteria cells, biomarkers, and proteins by changing spatial conformation, stacking aromatic rings, van der Waals interactions, electrostatic forces, and/or hydrogen bonding (Jarczewska et al., 2016). Aptamers are selected *in vitro* via the systematic evolution of ligands by exponential enrichment (SELEX) technique. When aptamers are used for ligand-specific biosensors that have two major components of a biological receptor such as an aptamer and a transducer for the detection (Fig. 1) (Duan et al., 2016), they are also called aptasensors (Munzar et al., 2019). Aptasensors have been utilized in various fields such as food safety surveillance, environmental contamination investigation, clinical diagnosis, and cancer prediction (Zuo et al., 2013; Wei et al., 2018; Dou et al., 2016a). For instance, we have developed multiple aptasensors for point-of-care (POC) detection of intact foodborne pathogens, such as *Salmonella enterica*, *Escherichia coli*, and *Listeria monocytogenes*, based on fluorescence detection (Zuo et al., 2013), and visual quantitative detection using a bar-chart microfluidic chip (Wei et al., 2018), respectively.

In addition to the capabilities of individual components, novel properties and synergistic functionalities of biosensors derive from the combination of nucleic acid aptamers and nanomaterials (MOFs), owing to the formation of nanostructured biointerfaces (Tang et al., 2015). Combining nucleic acids with MOFs for biosensing has attracted researchers' attention due to the large specific areas and stable structures of MOFs. The uniform crystalline structure of MOFs is beneficial for high specific surface areas, allowing for a wide variety of DNA, RNA, and aptamers to attach to them. Furthermore, because of tunable pore sizes of MOFs, different kinds of nucleic acids with diverse specificity can be immobilized onto the surface or inside of MOFs. In addition to configuration diversification, MOFs provide countless opportunities for the linkage of analytes. Because of the diversity of MOFs and aptamers, a large variety of MOFs-based aptasensors have been developed and exhibited outstanding advantages, including high sensitivity, great selectivity, and great potential for miniaturization and visual detection. MOFs-based aptasensors have been applied in many fields such as clinical diagnostics, disease treatment, POC testing, and environmental contamination surveillance (Mishra et al., 2018; Xie et al., 2015; Luo et al., 2019; Qiu et al., 2020).

Therefore, this article reviews recent advances of aptamer-functionalized MOFs-based biosensors. We first briefly introduce major MOFs' functionalization methods with aptamers. Then, we summarize the advances of aptamer-functionalized MOFs-based biosensors in different areas in terms of MOF's roles as either a signal probe or as a carrier for loading signal probes, because MOFs can be used as a signal probe for various types of biosensors (e.g. electrochemical, optical, and photoelectrochemical biosensors, as shown in Fig. 1) for direct detection of molecules or as a carrier for loading signal probes. In addition, since stimuli-responsive materials attract substantial research interests, we also present the stimuli-responsive aptamer-functionalized MOFs for sensing. Furthermore, the recent microfluidics technology has emerged as a versatile platform for biosensing (Fig. 1), POC detection, environmental monitoring, drug delivery, tissue engineering, material synthesis, and other fields, due to its numerous advantages such as miniaturization, high portability, low cost, rapid analysis, low reagent consumption, high throughput, customized design, and the compatibility to integrate different biosensors on a chip (Dou et al., 2017a; Sanjay et al., 2018; Tavakoli et al., 2019a; Dou et al., 2015; Sanjay et al., 2015; T. Sanjay et al., 2016a; Fu et al., 2020; Zhou et al., 2020a; Fu et al., 2018; Cheng et al., 2020; Wei et al., 2018; Dou et al., 2016b). Therefore, the integration of MOFs with the microfluidic technology for sensing is also reviewed, before we summarize current challenges and future perspectives on MOFs-based aptasensor at the end of this article.

2. Immobilization of aptamers on MOFs

Achieving efficient immobilization of aptamers or other nucleic acids on MOFs is an essential step to bridge MOFs with aptamers for subsequent biosensing. Meanwhile, immobilized aptamers can enhance MOFs' biocompatibility, dispersibility, and sensing properties. Immobilization of aptamers on MOFs can be achieved by covalent and non-covalent binding methods (Tolentino et al., 2020).

2.1. Introduction of MOFs and major categories

The concept of MOFs was first proposed by the group of O.M. Yaghi in 1995 (Yaghi et al., 1995). After these two significant MOFs were reported: MOF-5 (Li et al., 1999) and HKUST-1 (HKUST = Hong Kong University of Science and Technology), MOFs garnered much attention and were gradually applied in gas/energy storage, catalysis, sensing,

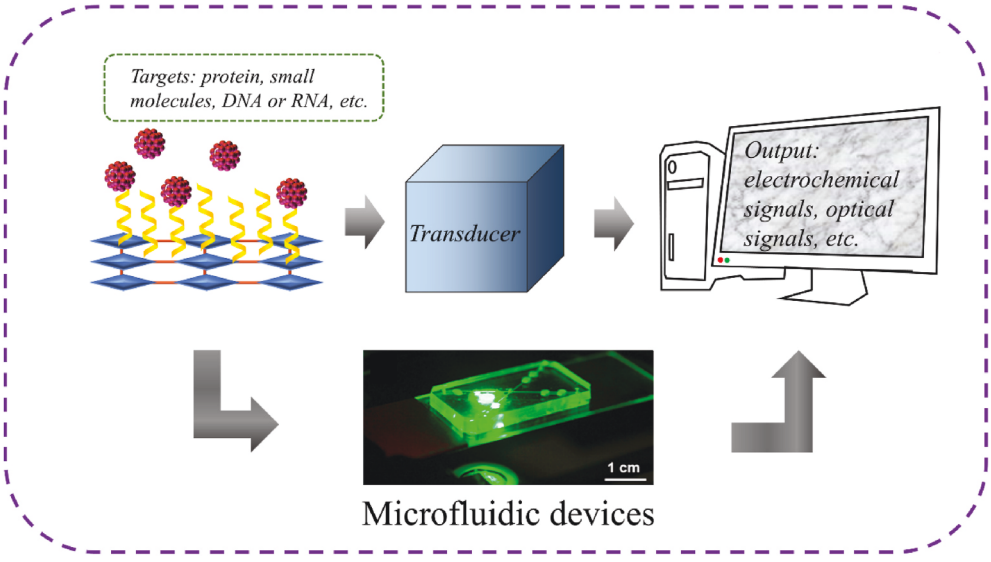

Fig. 1. Schematic of aptamers-functionalized MOFs-based and microchip biosensors. The photograph of the microfluidic device is reproduced with permission from (Dou et al., 2017a).

drug delivery, and separation. Through the extension and modification of terephthalic acid ligands, Yaghi et al. successfully synthesized a number of linear dicarboxylic acid ligands. These ligands were used to construct IRMOF (Isoreticular Metal-organic Framework), which had a similar topology to MOF-5 with tunable pore sizes in 2002 (Eddaoudi et al., 2002). In 2004, they synthesized MOF-177 with a specific surface area of 4500 m^2/g and excellent stability, which broadened the application to adsorption (Chae et al., 2004). In 2005, Ferey et al. combined synthetic chemistry with computer simulation and successfully synthesized MIL (Materials of Institute Lavoisier) MOFs, including two typical representatives, MIL-100 (Llewellyn et al., 2008) and MIL-101 (Férey et al., 2005). They demonstrated that both MIL-101 and MIL-100 have mesoporous cages with two different diameters of 2.9 nm and 3.4 nm for MIL-101, and 2.5 nm and 2.9 nm for MIL-100 by simulation, with corresponding high specific surface areas of 5900 m^2/g and 3100 m^2/g, respectively. Due to high chemical and thermal stability, both MOFs are widely used in catalysis. Differing from the synthesis methods mentioned above, Yaghi et al. reported a series of MOFs consisting of nitrogen-containing organic ligands through stirring at room temperature, which were called ZIF (Zeolitic Imidazolate framework) (Park et al., 2006). The new synthesis method provided a more straightforward operation process, which promoted widespread applications of MOFs in catalysis, sensing, and separation. Constructed by zirconium ions and carboxylic acid ligands, UIO (University of Oslo) and PCN (Porous Coordination Network) MOFs, UIO-6X (Cavka et al., 2008), and PCN-222 (Feng et al., 2012) are the most commonly used ones. As time goes by, more materials including metal ions and organic ligands are utilized to construct novel MOFs. Until now, a great number of papers have been published regarding MOFs' synthesis methods and applications. Since conventional MOF synthesis methods are not the focus of this review, please refer to other review articles for more details (Safaei et al., 2019; Kang et al., 2019). Researchers are devoted to exploring simpler strategies to construct MOFs and overcome the drawbacks of MOFs for more broad applications.

2.2. Covalent binding functionalization

The covalent immobilization methods often depend on amide bonds forming between an organic ligand on MOFs and nucleic acids. Since covalent binding is very stable, it is desirable for high-sensitivity biosensing. Li et al. reported an aptamer-MOFs composite for simultaneous detection of let-7a and miRNA-21. The functionalized MOFs were prepared by using porous UIO-66-NH_2 as a nanocontainer to load electroactive dyes and dsDNA as a gatekeeper to cap MOFs. The sensing platform was based on formation of an amide bond between the amino groups on the organic ligands of UIO-66 and the carboxyl groups on the end of aptamers (Fig. 2a) (Chang et al., 2019). Similarly, covalent crosslinkers are often introduced to link different functional groups on organic ligands and aptamers to achieve the covalent binding between them. For instance, Rouge et al. reported a covalent approach to bind DNA with MOFs indirectly. They assembled cross-linking of the surfactant, cetyltrimethylammonium bromide (CTAB), around ZIF-8, followed by attaching either thiol-terminated crosslinkers or diazido crosslinkers to the alkyne modified surfactant, which formed the surface-crosslinked micelle (SCM). Then, thiolated DNA was added to the alkyne-modified surface and immobilized on the SCM through a reaction between alkynyl and sulfhydryl. The method was used for the controlled release of small molecules and proteins from MOFs (Fig. 2b) (Tolentino et al., 2020). Li et al. fabricated a nanoprobe based on nanoscale MOFs for multicolor detection of DNA with high sensitivity and selectivity. Thiolated DNA covalently bonded to the surface of MOFs, which were modified with sulfosuccinimidyl 4-(N-mal-aminomethyl) cyclohexane-1-carboxylate (Sulfo-SMCC), acted as the covalent crosslinker (Wu et al., 2018). Additionally, Yuan et al. (Ma et al., 2015) immobilized the DNA Y-junctions on the surfaces of hollow Au nanocages through the aldimine condensation reaction by using glutaraldehyde (GA) as a crosslinker. Shahrokhian et al. reported another organic-inorganic nanomaterial amino-functionalized MOF as an electrochemical biosensor to detect *Escherichia coli* O157: H7 (Shahrokhian et al., 2018). GA was used as a cross-linking agent and promoted the formation of covalent bonds between GA and $–NH_2$ groups of PANI to bind functionalized MOFs with modified aptamers. Differential pulse voltammetry (DPV) was applied to this aptasensor for the monitoring and quantitation of the interaction between the aptamer and *E. coli* O157:H7 using methylene blue (MB) as an electrochemical indicator.

Additionally, the introduction of metal elements by MOFs enables alternatives to bind MOF with DNA through a covalent method. Mirkin and co-workers have studied the covalent binding of various MOFs and DNA. The series of UIO-66, PCN, and MIL-101 with active sites, were bonded to the phosphate groups on DNA and formed stable DNA-functionalized MOFs (Morris et al., 2014; Wang et al., 2017b). In 2019, Farha's group designed a new method for protein delivery based on the conjugation of DNA with MOFs to load proteins. Two water stable zirconium mesoporous MOFs, NU-1000 and PCN-222/MOF-545, were synthesized in a nanoparticle form. Next, the MOF NPs were surface functionalized with terminal phosphate-modified DNA to yield DNA-MOF NPs. The 3D oligonucleotide shell created a steric and electrostatic barrier to stabilize MOF NPs in high dielectric media and

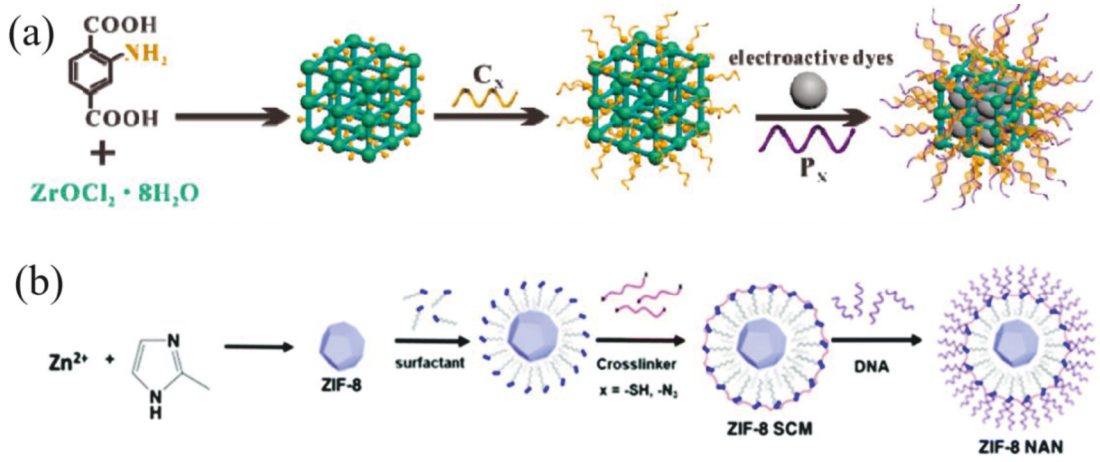

Fig. 2. Schematic of covalent binding between DNA and MOFs. (a) Amide bonds forming between amino groups on UIO-66 and carboxyl groups on the end of nucleic acids. Reproduced with permission from (Chang et al., 2019). (b) Covalent immobilization of nucleic acids with the aid of surfactant and crosslinkers. Reproduced with permission from (Tolentino et al., 2020).

rendered them functional with respect to cellular entry. The cellular uptake of proteins was enhanced due to the formation of Zr–O–P covalent binding, which originated from the terminal phosphate-modified oligonucleotides and the Zr center in MOFs (Wang et al., 2019a).

2.3. Non-covalent binding functionalization

Non-covalent binding is another way to bind MOFs and nucleic acids for biosensing. The non-covalent immobilization methods mainly depend on hydrogen bonding, electrostatic forces, and π-π interaction. These methods are easy to operate and do not affect the intrinsic structure and original properties of MOFs. Jiang et al. reported a method to directly detect DNA, in which a non-covalent method based on hydrogen bonds was used to bind DNA and MOFs. In their report, an amine-functionalized MOF, UIO-66-NH_2, had a conjugated π-electron system and offered the possibility of hydrogen bonds, allowing suitable interaction between MOFs and single-stranded DNA (ssDNA). With the simple functionalization process, the fluorescence biosensor was fabricated and used for the detection of DNA with a specific sequence, which can bind ssDNA by hybridizing complementary pairs (Zhang et al., 2014). Ding's group synthesized $[Y(L)(DMF)_{0.75}]_n$ (Y-MOF) (H_3L = terphenyl- 3,4″,5-tricarboxylic acid; DMF, dimethylformamide) as a ratiometric fluorescent biosensor for the detection of C-reactive protein autoantibody (CRP Ab) with high sensitivity. Fluorescein amide (FAM)-labeled NH-ssDNA was employed to construct the scarcely reported hybrid FAM-labeled NH-ssDNA/Y-MOF sensing platform through hydrogen-bonding interactions (Wang et al., 2020). Moreover, similar π-π interaction strategies have been reported to construct sensing platforms for the detection of biomolecules (Zhang et al., 2018). Through the π-stacking and hydrophobic interactions, Cu-MOF and nucleobases can be linked. Jiang et al. demonstrated a biosensor for simultaneous detection of three conserved sequences of Zika virus RNA sequences. The biosensor was fabricated based on Cu-based MOFs, which interacted with dye-tagged ssDNA through the π-π force. The MOFs-based biosensors have high selectivity, sensitivity, and low limits of detection (LODs) of 0.56 ± 0.02, 0.16 ± 0.04, and 0.19 ± 0.05 nM, respectively (Xie et al., 2019). Likewise, Cu-BTC MOFs (H_3BTC = benzene-1,3,5-tricarboxylic acid) were chosen to bind DNA non-covalently to fabricate biosensors because of the conjugated π-electron of H_3BTC ligands. The as-prepared biosensor was able to detect trinitrophenol, gaseous formaldehyde, and glyphosate (Wang et al., 2018a; Gao et al., 2018; Cao et al., 2019).

In some cases, more than one form of non-covalent interactions may exist in the combination of DNA, RNA, or aptamers with MOFs. Zhang's group reported a straightforward method for the detection of miRNA using quartz crystal microbalance (QCM) (Ma et al., 2020). They used a series of UIO-66 with different zeta potentials to investigate the bonding principles in detail. They concluded that the interactions between UIO-66 and let-7a (a type of miRNA) included π stacking, electrostatic interactions, hydrogen-bonding, or Zr–O bonds. The combination of covalent and non-covalent interactions can provide stronger binding forces for nucleic acids to attach more firmly to the MOF surface.

3. MOFs as signal probes for aptasensing

As we have stated earlier, MOFs exhibit excellent optical, catalytic, and electrochemical activities due to the diverse compositions of metal and organic ligands. Therefore, MOFs can produce signals directly for detection in an aptamer-based biosensing system. This section introduces different kinds of biosensors by using MOFs as signal probes, as summarized in Table 1.

3.1. MOFs-based optical aptasensors

MOFs-based optical aptasensors with an optical transducer system are widely used in biosensing, which generally include four types of optical aptasensors: fluorescence, chemiluminescence, electrochemiluminescence, and colorimetric aptasensors. The intrinsic optical properties of MOFs are essential for the generation of luminescence signals. MOFs can be utilized as luminescence signal probes directly or as signal quenchers in different detection platforms. In this section, various MOFs-based optical aptasensors and their corresponding properties are introduced.

Fluorescence resonance energy transfer (FRET) is a non-radiative energy transfer phenomenon appearing in an environment for which a fluorescent donor and a light-absorbing acceptor are required (Neema et al., 2020). FRET can occur on condition of the proximity where the donor and the acceptor are within a range of <10 nm and have sufficient spectral overlap (Ganiga and Cyriac, 2016). Feng et al. introduced a fluorescent aptasensor based on terbium (III) metal-organic frameworks (Tb-MOFs) and PDDA (poly-dimethyl dialyl ammonium chloride)-aggregated-AuNPs for chlorpyrifos (CPF) detection (Liu et al., 2019a). Tb-MOFs were used as fluorescence probes to provide the optical signal. In the presence of dispersed AuNPs, the emissions of Tb-MOFs can be quenched by FRET while the PDDA-aggregated AuNPs have little effects on quenching FRET. Hence, fluorescence can be detected in the presence of aggregated AuNPs, and fluorescence signals can be used to detect targets that can cause the status change of AuNPs. In this work, the aptamer interacted with PDDA via electrostatic interaction to prevent the aggregation of the AuNPs. The developed FRET-based aptasensor showed a wide linear range of 5–600 nM for CPF detection with the LOD of 3.8 nM. The assay was selective for CPF over other interfering compounds including carbofuran (CBF), dichlorphos (DCP), phoxim (PHX), and acetamiprid (AMP). The method was successfully applied for the determination of CPF spiked in tap water, vegetables and fruits samples. The mean recoveries of CPF range from 87.90% to 93.60% for tap water and 82.60%–90.70% for cucumber, respectively.

MOFs can be used as quenchers to affect fluorescent signals for biosensing. Dang et al. designed an aptasensor based on two-

Table 1
MOFs-based optical aptasensors by using MOFs as signal probes.

Type of MOFs	Target	Functionalization methods	Linear range	Detection limit	Ref
Tb-MOFs	CPF		5–600 nM	3.8 nM	[(Liu et al., 2019a)]
H_2dtoaCu	ATP	π-π stacking and hydrogen bond	25–400 nM	8.19 nM	[(Hai et al., 2018)]
MIL-101	Thrombin	π-π stacking		15 pM	[(He et al., 2017)]
	OTC			4.2 nM	
Cu (HBTC)-1	OTC	Amidation reaction	0.50–5.00 μg/L	0.40 μg/L	[(Tan et al., 2020)]
Cu-TCPP	CAP		0.001–10 ng/mL	0.3 pg/mL	[(Yang et al., 2018)]
MIL-100 (Fe)	AFP	Electrostatic interaction	1.0×10^{-10} - 3.0×10^{-5} g/L	7.7×10^{-11} g/L	[(Han et al., 2020)]
Cu-TCPP	thrombin	Au–S bond	8.934×10^{-13} - 5.956×10^{-10} M	2.178×10^{-13} M	[(Lin et al., 2020)]
Cu-MOFs	α-syn	Au–S bond	2.43 fM - 0.486 pM	0.42 0.38 fM	[(Wu et al., 2020a)]
			1.39 fM - 0.243 pM		
Ru@ MOFs	amyloid-β (Aβ) protein		10^{-5} - 500 ng/mL	3.9 fg/mL	[(Wang et al., 2019b)]
Fe-MIL-88	PSA	Au–S bond	0.5–500 ng/mL	0.058 ng/mL	[(Shao et al., 2018)]
Fe-MIL-88NH_2	KANA	Pt–S bond	0.0005–30 ng/mL	0.2 pg/mL	[(Luan et al., 2017)]

dimensional (2D) sheet MOFs of N, N-bis(2-hydroxyethyl)dithiooxamidato copper (II) (H_2dtoaCu) for the fluorescence detection of adenosine triphosphate (ATP) (Hai et al., 2018). The FAM-labeled ATP aptamers were first adsorbed onto the surface of H_2dtoaCu MOFs strongly via π-π stacking and hydrogen bond interactions between the nucleotide bases and the H_2dtoaCu surface. Owing to photoinduced electron transfer (PET), the emissions of FAM-labeled ATP aptamers were successfully reduced. In the presence of ATP, the FAM-labeled ATP aptamers specifically formed ATP-binding aptamer complexes that had weaker adsorption and separated from the H_2dtoaCu surface, resulting in the recovery of fluorescence (Fig. 3a). This aptasensor exhibited an excellent linear relationship in the range of 25–400 nM ATP with a LOD of 8.19 nM. To determine the selectivity of H_2dtoaCu, GTP, UTP, TTP and CTP were also included in the investigation. As a result, the fluorescence intensity was stronger than the four analogs when ATP existed. To improve detection sensitivity, Li et al. reported a fluorescence aptasensor using a fluorescence amplification strategy (He et al., 2017). MIL-101 was used to serve as a quencher to quench fluorescence emissions, while the release of the aptamers was used as fluorescence providers from MIL-101 due to binding with targets and resulted in fluorescence recovery. Under the influence of RecJf hydrolysis, the targets were free from aptamers once aptamers were fractured, and then conjugated, while bringing away other aptamers from MIL-101. After many cycles, the fluorescence signal was finally amplified significantly. The LODs were 15 pM and 4.2 nM for OTC (oxytetracycline). These are two orders of magnitude lower than that of a conventional homogeneous fluorescence assay. The linear ranges were 0.05–100 nM and 10–2000 nM for thrombin and OTC, respectively. In 2019, Zhao et al. also developed a fluorescence aptasensor using 2D MOFs as a quencher for the detection of OTC (Tan et al., 2020). They solved a tricky problem of low sensitivity in fluorescence detection as well. The fluorescence background was reduced due to the covalent linkage of DNA probes to MOF nanosheets. Specifically, a short-chain DNA probe and surface passivation improved fluorescence efficiency. Upon the addition of OTC, aptamers bound with OTC and short-chain DNA probes were released to generate signals. The aptasensor exhibited superior detection performance for OTC with a linear range of 0.50–5.00 μg/L and a low LOD of 0.40 μg/L. In addition, Gan et al. developed another aptasensor based on a 2D MOF (Cu-TCPP nanosheets) (TCPP, tetrakis (4-carboxyphenyl) porphyrin) and FRET (Yang et al., 2018). Cu-TCPP was employed for circular strand replacement DNA polymerization (CSRP) and used as a quencher for signal amplification. SYBR Green I (SG) was used to produce fluorescence signals for target quantification. Due to the quenching properties of 2D MOF, the team also proposed multicolor fluorescence (Yang et al., 2019) probes for simultaneously detecting various analytes in biological samples. They used Y junction DNA (Y-DNA), ssDNA, and different targets (i.e. chloramphenicol (CAP), OTC, and kanamycin (KANA)) to fabricate a delicate reaction cycle. The dye-decorated ssDNA could leave Cu-TCPP nanosheets and fluorescence remarkably enhanced. The low LODs of 1.5 pM CAP, 2.4 pM OTC, and 1 pM KANA were achieved. The linear ranges were 0.005–10.0 nM for CAP, 0.008–50 nM for OTC, and 0.003–30 nM for KANA, respectively.

Chemiluminescence immunoassay (CLIA) is popular in molecular detection due to its high luminescence efficiency and low detection limit (Fonseca et al., 2019). However, it also has some disadvantages such as low photostability, poor biocompatibility, and biotoxicity, which limit its broader application (Liu et al., 2020). Recently, to conquer its drawbacks and expand the scope of application, researchers fabricated various MOFs and applied them in chemiluminescence (CL) biosensors to improve overall performance. In a MOFs-based CL biosensor, MOFs can be used as a catalyst to produce or affect the CL signals. For instance, Luo et al. established a chemiluminescent sensing platform based on the luminol–H_2O_2–MOF system to detect α-fetoprotein (AFP) (Han et al., 2020). In this system, AFP-aptamer was used as a target recognition element, and MIL-100 (Fe) with peroxidase-like catalytic activity was used as the catalyst. In the presence of H_2O_2 and luminol, AFP induced aptamer conformational changes to stimulate the generation of CL. This aptasensor exhibited a wide dynamic range of 1.0×10^{-10} g/L to 3.0 ×

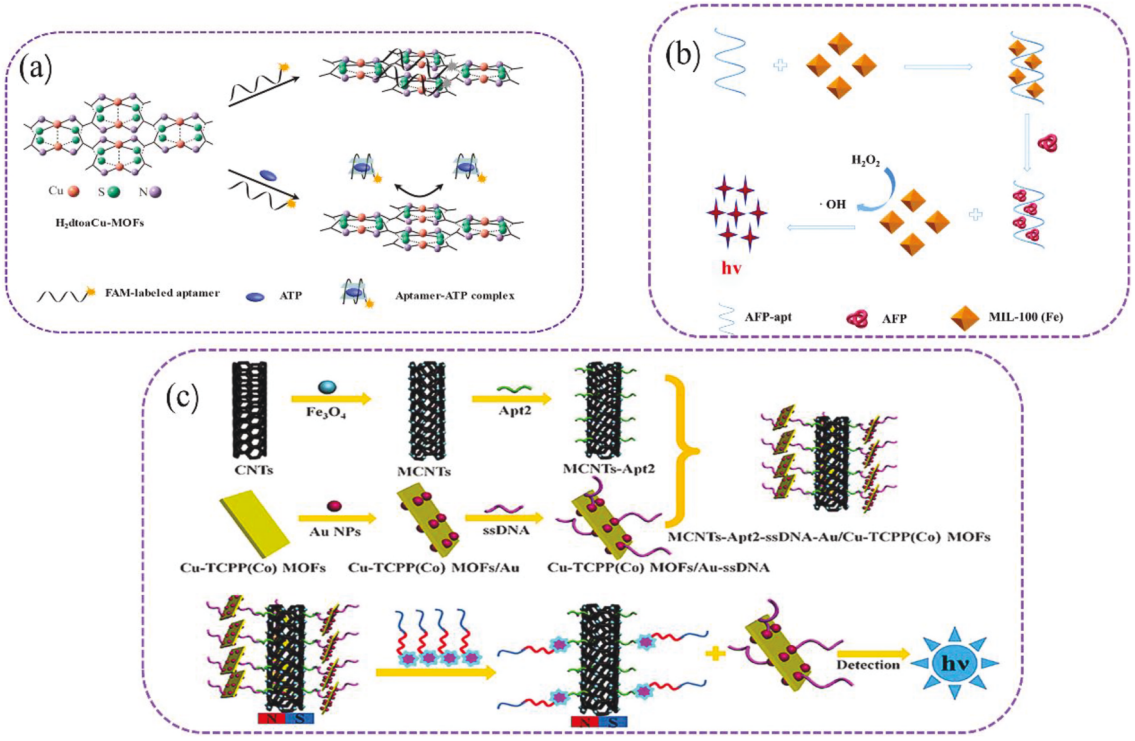

Fig. 3. Schematic of MOFs-based fluorescence and CL aptasensors. (a) A fluorescence aptasensor based on fluorescence quenching on H_2dtoaCu to detect ATP. Reproduced with permission from (Hai et al., 2018). (b) A chemiluminescent sensing platform based on the luminol–H_2O_2–MOF system. Reproduced with permission from (Xie et al., 2019). (c) A preparation process of Cu-TCPP (Co) MOFs based CL aptasensors. Reproduced with permission from (Ma et al., 2020).

10^{-5} g/L and high sensitivity with a LOD of 7.7 × 10^{-11} g/L. Several interfering agents were added together with AFP for determining the selectivity, including bovine serum albumin (BSA), carcinoembryonic antigen (CEA), prostate specific antigen (PSA), glucose, adrenaline, carbamide, Na^+, and K^+. Eight measurements were performed and the relative standard deviation (RSD) of the values was 2.7%, indicating good repeatability. The signal decrement was only 5.7% after 21 days, implying high stability (Fig. 3b). Wang's group introduced a CL aptasensor based on 2D MOFs in the luminol CL environment (Lin et al., 2020). 2D MOFs exposed more active sites and provided excellent catalytic efficiency when compared to original MOFs. In their report, they used Cu-TCPP (Co) MOFs for thrombin detection. Afterward, the Cu-TCPP (Co) MOFs/Au-ssDNA composites were replaced by thrombin owing to the stronger binding force between aptamer with thrombin than aptamer with ssDNA. The reaction of the luminol CL system would be catalyzed by Cu-TCPP(Co) MOFs and provide a "signal-on" CL

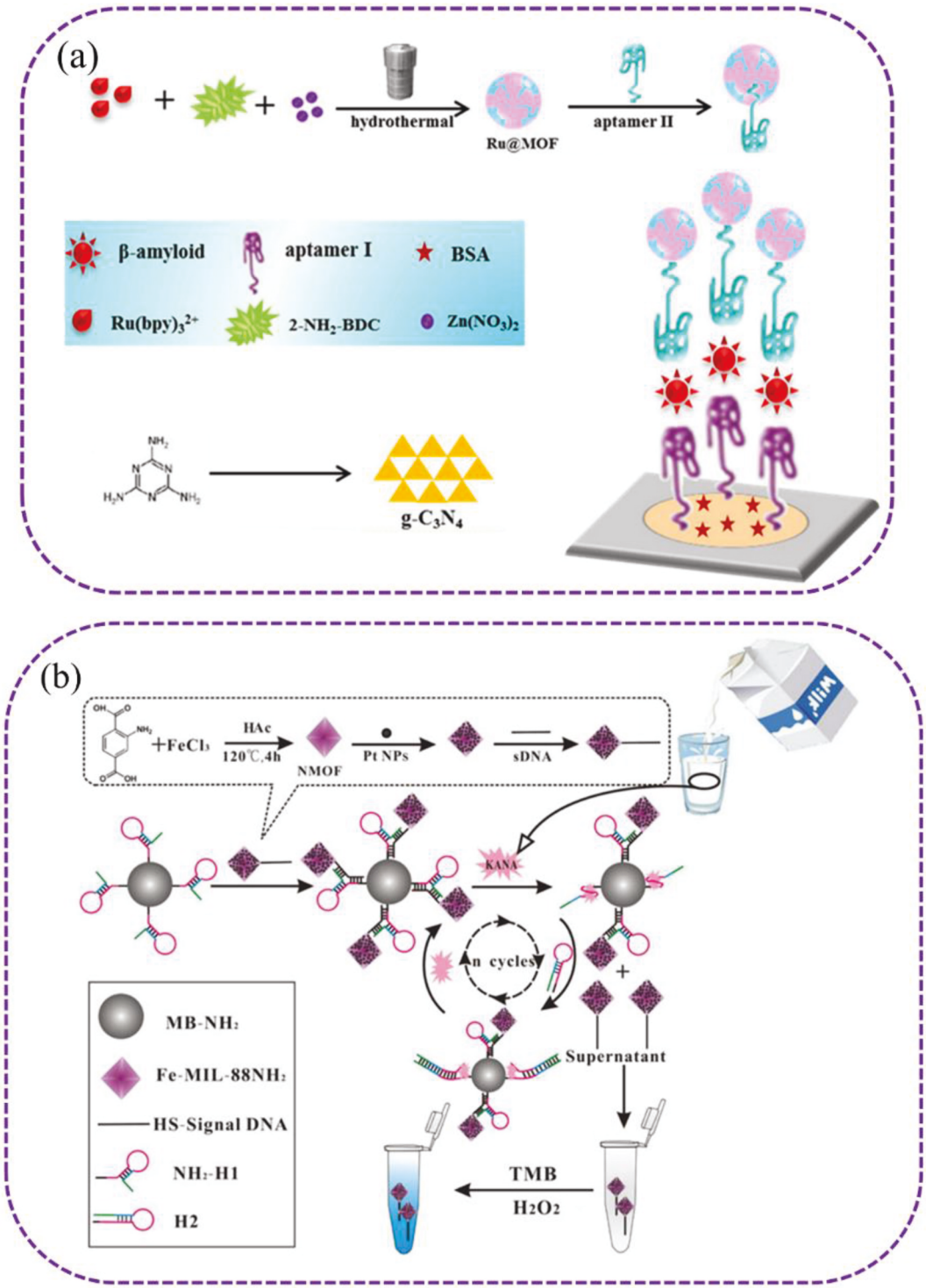

Fig. 4. Schematic illustrations of ratiometric ECL aptasensors and colorimetric aptasensor. (a) Ru-MOFs based ratiometric ECL-RET aptasensor using Ru-MOFs and carbon nitride nanosheet (g-C_3N_4 NS). Reproduced with permission from (He et al., 2017). (b) Mimicking enzyme-based colorimetric aptasensor composing of Fe-MIL-88NH_2. Reproduced with permission from (Luan et al., 2017).

mechanism. The biosensor achieved a LOD as low as 2.178×10^{-13} mol/L, with a linear range from 8.934×10^{-13} to 5.956×10^{-10} mol/L. The selectivity of this aptasensor was measured via detecting 5-hydroxytryptamine, serum albumin, lysozyme, glucose and epinephrine, which yielded negligible signal responses compared to thrombin (Fig. 3c).

Electrochemiluminescence (ECL) has garnered a lot of interest in clinical diagnosis, molecule detection, and biosensing due to its high sensitivity, low background signal, and simple design (Li et al., 2012a). Luminol (Liu et al., 2016), Ru $(bpy)_3^{2+}$(Feng et al., 2016), and quantum dots (QDs) (Ma et al., 2015) are widely used as luminophores in ECL. MOFs in ECL aptasensors usually serve as catalysts or quencher of emitters. For example, in Tu's work, AuNPs@MOFs promoted strong emission for luminol, providing the potential for the detection of alpha synuclein (α-syn) oligomer, a biomarker for the early diagnosis of Parkinson's disease. When α-syn oligomer existed, the reduction of ECL emission occurred owing to its large steric hindrance. The changed ECL signals were used for α-syn detection with the LOD of 0.4 fM and the linear range of 2.43 fM to 0.486 pM (Wu et al., 2020a). Although luminophores could theoretically be directly utilized without signal promoters, nanomaterials such as MOFs can play an important role in ECL aptasensing due to the imperative step of signal amplification. The team of Jia designed a ratiometric electrochemiluminescence resonance energy transfer (ECL-RET) aptasensor using Ru-MOFs and a carbon nitride nanosheet (g-C_3N_4 NS) as energy donor-receptor pairs to detect Aβ protein (Wang et al., 2019b). Ratiometric aptasensors can be a promising design that promote accuracy and sensitivity via avoiding the influence from background signals. These donor-receptor pairs were firstly applied for the detection of Aβ protein. With the addition of Aβ, the Ru-MOF anode ECL increased, whereas the cathode ECL of g-C_3N_4 NS decreased. MOFs also served as signal enhancers by loading abundant amounts of luminophores Ru $(bpy)_3^{2+}$ and driving the conversion from $S_2O_8^{2-}$ to $SO_4^{\bullet-}$. The proposed aptasensor exhibited a wide linear range from 10 fg/mL to 500 ng/mL, with the LOD as low as 3.9 fg/mL. The ECL intensity did not significantly change with the addition of some interfering agents such as CA15-3, CA19-9, CEA, and mixtures, and received similar signals provided by 0.01 ng/mL Aβ protein, compared to blank samples. The repeatability was good, as manifested by the RSD of 2.37% in detecting six samples of Aβ (0.01 ng/mL). In real human serum, the recovery rates were between 99.2 and 103%, showing good accuracy for clinical diagnosis and potential for practical applications (Fig. 4a). Han et al. established another ratiometric ECL aptasensor using Fe-MIL-88 as not only a quencher but also an enhancer (Shao et al., 2018). They introduced QDs and luminol as ECL emitters. MOFs assisted the ECL of luminol and quenched the ECL of QDs. Before prostate-specific antigen (PSA) was added, the signal of luminol was turned on. Meanwhile, the signal of QDs was quenched by Fe-MIL-88. After PSA was added, the signals conversed owing to the increasing distance between Fe-MIL-88 and electrodes. The linear range for PSA detection was from 0.5 to 500 ng/mL and the LOD was 0.058 ng/mL.

Colorimetric biosensors possess some advantages of low costs, but the sensitivity is not high (Liu and Lu, 2003; Nath and Chilkoti, 2002). Among different colorimetric assays, 3,3′,5,5′-tetramethylbenzidine (TMB) is widely used as the colorimetric substrate (Fu et al., 2018; Zhou et al., 2020b). In 2017, Gan's group reported a colorimetric aptasensor for KANA detection. This method used Fe-MIL-88NH_2–Pt (NMOF-Pt-sDNA) as signal tags, which have great peroxidase-like activities, to catalyze non-colored TMB into blue-colored oxidized TMB (oxTMB) (Luan et al., 2017) (Fig. 4b). By using a UV–vis spectrophotometer, the aptasensor exhibited a LOD of 0.2 pg/mL and a linear range of 0.0005–30 ng/mL. The specificity was verified by utilizing five other antibiotics, amino acids, proteins and metal ions as interfering agents. Gan et al. fabricated a colorimetric aptasensor for the detection of antibiotics using CAP as a model in 2018 (Luan et al., 2018). They used Fe-MIL-88-Pt as the peroxidase mimic signal tag. MIL-88, DNAzyme, and Pt in the tag offered peroxidase mimic activity to catalyze TMB with H_2O_2 into oxTMB. With the recycle amplification strategy, numerous MOFs were released to catalyze TMB, resulting in color development. The constructed aptasensor for the detection of CAP exhibited a wide linear range of 0.1 pM (0.0323 pg/mL) - 1000 pM (323 pg/mL) and a LOD of 0.03 pM (0.0097 pg/mL). Moreover, the reproducibility of the designed colorimetric aptasensor was evaluated with the RSD of 1000 pM CAP for six times, and the obtained RSD was about 2.15%. In addition, in order to verify the practical performance of the aptasensor, five different types of milk samples were employed for CAP detection. The recoveries in five milk samples were between 90.0% and 120%. Other nanomaterials such as Fe_3O_4 NPs and AuNPs also have peroxidase mimic activities and are often used to catalyze TMB as well as for biosensing with colorimetric, temperature, or other detection modes (Zhou et al., 2020b; Fu et al., 2018).

3.2. MOFs-based electrochemical aptasensors

For MOFs-based electrochemical biosensors, MOFs have two main approaches to provide electrochemical signals. One approach depends on its intrinsic characteristics, such as catalysts for redox reactions to provide electrochemical signals. Not only can some metal ions on MOFs be catalyzed near an electrode for signal amplification, but also active substances in solutions. The other approach is to utilize MOFs to decrease impedance. Once targets conjugate onto aptamers immobilized on MOFs, impedance sharply increases, thus forming signal changes to reflect the successful application of developed aptasensors (Gu et al., 2020). Based on these two strategies, more electrochemical sensors have been created, and the sensitivity and stability of detection have been improved. This provides a solid foundation for the use of electrochemical sensing in clinical diagnosis. Lei et al. proposed an innovative nucleic acid biosensor by using pristine MOFs as the electrochemical signal nanoprobe. They prepared PCN-222, one kind of MOFs with electrocatalytic activity, by using porphyrin as a linker. The PCN-222 could generate electrocatalytic current through the catalysis of oxygen reduction. The biosensor was prepared by immobilizing triple-helix DNA on a glassy carbon electrode (GCE) modified with graphene. In the presence of the target DNA, its recognition with an assistant DNA triggered the Exo III cleavage process, accompanied by the target recycling and the release of the hairpin DNA. The porphyrinic MOF-based aptasensor with the enhanced current was used to detect target DNA in complex serum matrix with a LOD of 0.29 fM and a wide linear range from 10 fM to 100 nM, which showed great potential for detection of complex samples. Good repeatability of the biosensor was achieved via examining the target DNA concentrations of 50 fM, 50 pM and 20 nM with the RSDs of 2.5%, 4.3% and 3.1%, respectively (Ling et al., 2015). However, the signal MOFs were micrometer-sized crystals and not beneficial for the electrocatalytic efficiency, which affected the detection sensitivity. Therefore, the researchers used a DNA recycling amplification method to improve sensitivity with the aid of exonuclease, which increased operational difficulty and cost.

Many kinds of MOFs-based composites have been designed and prepared as signal probes to fabricate aptasensors. Lu et al. presented an aptasensor utilizing Zr-MOF-on-Zn-MOF as signal tags. Owing to hydrogen bonding, electrostatic interactions, and π-π stacking, aptamers were tightly stabilized onto Zr-MOFs with nontoxicity. With the excellent affinity towards nucleic acids, Zn-MOF was used to immobilize G-quadruplex formed by aptamer strands and the target, protein tyrosine kinase-7 (PTK7), proving a promising strategy for analyte detection. They found that the order of adding organic ligands and petal precursors influences the morphology and properties of obtained materials (Zhou et al., 2019a). This proposed aptasensor provided ultralow LODs of 0.84 and 0.66 pg/mL, as obtained by electrochemical impedance spectroscopy (EIS) and DPV, respectively. The linear range for PTK7 detection was from 1.0 pg/mL to 1.0 ng/mL. Recently, a label-free aptasensor was constructed based on a bimetallic ZnNi MOF with a molar ratio of 1:2, which exhibited better electrochemical performance of nanocomposites' adsorption of Ni^{2+} to aptamers and the synergistic effect of Zn^{2+}/Ni^{2+} in

MOF matrixes compared to other ratios (Tian et al., 2020). Using this aptasensor, a wide linear range of 0.0001–100 ng/mL and a low LOD of 20.32 fg/mL were achieved for the detection of adenosine (AD). Zhou's group developed an electrochemical aptasensor based on Co-MOF and terephthalonitrile-based covalent organic framework (TPN-COF) (Liu et al., 2019b). This nanocomposite has large specific areas and nitrogen-rich groups, resulting in excellent electrochemical activities. Owing to hydrogen bonds and π-π stacking interactions, aptamers were bound to nanocomposites non-covalently for the detection of ampicillin (AMP). Using an EIS detection method, this aptasensor demonstrated a wide linear range (1.0 fg/mL-2.0 ng/mL) and a low LOD of 0.217 fg/mL.

Furthermore, Wang et al. designed nanohybrids of Ce-MOF and COF (MCA) (melamine and cyanuric acid) for OTC detection (Zhou et al., 2019b). They first synthesized a series of Ce-MOF@MCA hybrids with diverse amounts of MCA layers embedded within Ce-MOF. By comparing different OTC aptasensors based on Ce-MOF@MCA with different amounts of MCA, the nanohybrid with higher sensitivity and a lower LOD was selected. The nanohybrid combined advantages of Ce-MOF and MCA and showed strong bioaffinity toward aptamers. The OTC concentration range was 0.1–0.5 ng/mL under optimal conditions, and the low LOD was 17.4 fg/mL. The reproducibility of the fabricated electrochemical aptasensor was tested and RSD was around 1.16%. To investigate the feasibility of the proposed aptasensor, it was used to detect OTC in various aqueous solutions, including milk, wastewater, and urine. The achieved recoveries were 101.9–113.6%, 94–103.7%, and 92.6–106.5% in milk, river water, and urine, respectively. Zhou et al. used an Au–Cu-MOF as a signal probe and gold nanoparticles-reduced graphene oxide (Au-rGO) as a substrate for the electrochemical detection of acetamiprid with high sensitivity (Qiao et al., 2019). Au-CuMOF was used to label the probe DNA (pDNA), while Au-rGO with a high specific surface area and excellent conductivity was bound to complementary strand DNA (cDNA). They studied the electrochemical behavior of CuMOF and drew a conclusion that CuMOF serves as an ideal candidate in electrochemical detection. The linear range of this proposed electrochemical aptasensor was 0.1 pM–10.0 nM and the detection limit was as low as 2.9 fM. The reproducibility was evaluated by measuring 1.0 nM acetamiprid samples with five electrodes fabricated independently under the identical reaction conditions. RSD was 1.71%, indicating good reproducibility of the proposed aptasensor. In addition, after the aptasensor was kept in a refrigerator at 4 °C for two weeks, over about 97% of the original current response was still retained, confirming that the aptasensor had high stability at 4 °C, though the stability at room temperature is not clear. The aptasensor was used for acetamiprid detection in tea samples. It was noticed that the recovery range was between 96% and 104%.

By using the impedance decreasing strategy, Du and co-workers demonstrated an electrochemical aptasensor by using bimetallic MOFs as a signal probe for the detection of carbohydrate antigen 125 (CA125) and living breast cancer (MCF-7) cells (Wang et al., 2019c) (Fig. 5a). In this work, two kinds of bimetallic TbFe-MOFs were designed by a MOF-on-MOF strategy and utilized as a platform to anchor the CA125 aptamer for the detection of CA125 and MCF-7 cells. When the targets were recognized and immobilized onto MOFs, the impedance changed, which could be detected for sensing. The Tb-MOF-on-Fe-MOF nanoarchitecture demonstrated superior biocompatibility and good endocytosis. The developed aptasensor provided satisfactory LODs of 58 μU/mL and 19 cell/mL from EIS and cyclic voltammetry (CV), respectively. Moreover, 500, 5000 and 100000 cell/mL of MCF-7 cells were utilized in five tests via the same MOFs for exploring reproducibility. The RSDs were 3.31%, 3.98% and 1.76%, respectively, indicating acceptable

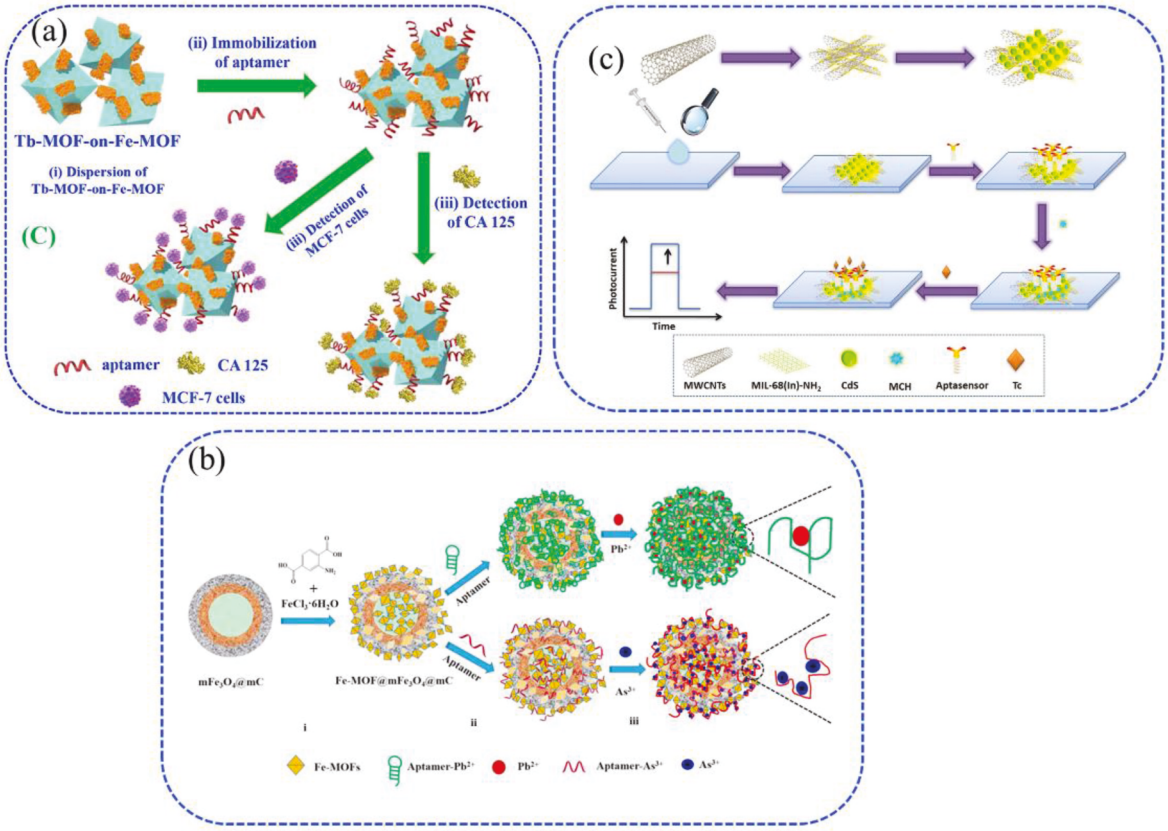

Fig. 5. MOFs-based electrochemical aptasensors. (a) Electrochemical aptasensors using Tb-MOF-on-Fe-MOF for the detection of CA125 and living cancer cells. Reproduced with permission from (Wang et al., 2019c). (b) Fe-MOF-derived nanostructures for heavy ions detection. Reproduced with permission from (Zhang et al., 2017a). (c) MOFs-based PEC aptasensors. A label-free PEC biosensor constructed using MIL-68(In)–NH_2/MWCNT/CdS composites. Reproduced with permission from (Zhang et al., 2019a).

reproducibility. After 15 days, 97.7% of the initial response was obtained, showing good stability. To overcome the low electroactive characteristics of MOFs, various electroactive materials were assembled with MOFs to improve their properties. Chen et al. designed such a Ni-MOF, a sensitive and stable signal probe by interlacing with 4,4′, 4″-Tricarboxytriphenylamine (H_3TCA, a redox-active ligand as an electroactive source) and magnetic ordered Ni_4O_4 clusters as electronic transport nodes for the electrochemical detection of thrombin (Wu et al., 2019a). The active sites of TCA and well-organized magnetic Ni_4O_4 clusters assembled in the Ni-MOF improved the stability. This electrochemical aptasensor had high detection sensitivity, with the LOD of 0.016 pM and a linear range from 0.05 pM to 50 nM. Yuan et al. demonstrated a target-triggering nicking enzyme signaling amplification (NESA) strategy for thrombin detection (Yang et al., 2017a). This electrochemical aptasensor used Co-MOFs decorated with PtPd NPs (CO-MOFs/PtPdNPs) as a redox mediator. Hairpin DNA participated in the NESA strategy and was used to enhance the electrochemical signal, while MOFs acted as not only nanocarriers but also a redox mediator to avoid the addition of extra redox media. PtPd NPs also acted as an alternative of horseradish peroxidase (HRP) to improve the oxidation of H_2O_2, speeding up the conversion of CO^{2+} to CO^{3+}. All these strategies amplified the signal, leading to a low LOD of 0.32 pM. The dynamic range from 1 pM to 30 pM was fairly narrower than the previous work (Wu et al., 2019a). He et al. reported a DNA-PtNi@Co-MOF based electrochemical aptasensor, including $CoSe_2$/AuNRs and nicking enzyme for zearalenone (ZEN) detection (He and Yan, 2020). Due to the intrinsic catalytic ability towards thionine (Thi), this electroactive MOFs-based nanocomposite (PtNi@Co-MOF) can hybridize DNA on the substrate with the aid of ZEN-Apt (aptamer), resulting in enhanced current responses and a low LOD of 1.37 fg/mL (S/N = 3). In addition, Zare et al. introduced a label-free electrochemical aptasensor for aflatoxin M_1 (AFM1) measurement (Jahangiri-Dehaghani et al., 2020). By decorating PtNPs on MIL-101 (Fe), the electrochemical aptasensor exhibited strong sensitivity towards AFM1 due to the enhancement of MOFs' conductivity. The linear range was from 1.0×10^{-2} to 80.0 ng/mL, and the LOD was 2.0 pg/mL under optimum conditions towards AFM1 detection. These electrochemical aptasensors were implemented for AFM1 detection in pasteurized milk samples and powder. Combined reduced graphene oxide (RGO) or graphene oxide (GO) with Cu-MOF, Jalali et al. designed an electrochemical aptasensor based on Cu-MOF-RGO and Cu-MOF-GO. Cu-MOF-GO was modified on the electrode surface to enhance conductivity by reducing GO to RGO (Hatami et al., 2019). Cu-MOF-RGO also served as a signal tag and to immobilize the MUC1 aptamer. The formation of MUC1-aptamer complexes hindered electron transportation leading to signal decrement, and thus the signal decrease could be used for the target quantification. A linear range was obtained with a DPV method, which was 0.1 pM–10 nM (25 pg/mL-2500 ng/mL) with a LOD of 0.033 pM (7.5 pg/mL). He et al. fabricated a ZIF-8-Thi-Au-based electrochemical aptasensor for microcystin-LR (MC-LR) measurement (Wu et al., 2020b). MoS_2–PtPd was used to modify the electrode surface as a substrate to conjugate aptamers. The complementary strand of the MC-LR aptamer was loaded on the surface of ZIF-8-Thi-Au to bind ZIF-8-Thi-Au onto the electrode. MOFs acted as signal tags with high conductivity due to the presence of AuNPs, which increased the current signal together with Thi's redox reactions. By replacing the target with ZIF-8-Thi-Au, signal decrement indicated the increase of the target concentration. Under optimal conditions, the LOD was obtained as 0.006 ng/mL, along with a wide linear range of 0.01–50 ng/mL.

Conjugating diverse nanomaterials have aroused much attention for the performance improvement of MOFs-based sensors. Zhou et al. demonstrated a MOFs-based aptasensor with nanomaterials, abundant carbon dots (CDs), embedded within the cavities of bimetallic ZrHf-MOF (Gu et al., 2019). With structure stability, strong biocompatibility, and high electrochemical activity, CDs@ZrHf-MOF displayed higher electrochemical performance compared with isolated ZrHf-MOF. Using this aptasensor to detect human epidermal growth factor receptor-2 (HER2) and living HER2-overexpressed MCF-7 cells, they obtained the LOD of 19 fg/mL and 23 cell/mL, and the wide linear ranges were 0.001–10 ng/mL and 1×10^2–1×10^5 cell/mL, respectively. Zhou et al. synthesized UIO-66-2NH_2, a type of Zr-MOFs, by using the mixture of 2-aminoterephthalic acid and 2,5-diaminoterephthalic acid (DA) as ligands (Li et al., 2020). A phosphate group-modified aptamer (PO_4-Apt) was anchored on the prepared MOFs. Using these nanomaterials as electrochemical aptasensor to detect living cancer cells, the multicomponent UIO-66-2NH_2 showed high biocompatibility toward PO_4-Apt via covalent bonds of Zr–O–P and high electrochemical performance. For MCF-7 cells, the developed aptasensor showed an extremely low LOD of 31 cell/mL in a wide linear range from 100 to 100,000 cell/mL. Meanwhile, interference effects from possible proteins with different concentrations (0.1, 1.0, and 10 pg/mL) were tested using the aptasensor, including vascular endothelial growth factor (VEGF), AFP, epidermal growth factor receptor (EGFR), and IgG. Compared to the substantial signal of MCF-7, the electrochemical signals caused by the interferents were negligible. Moreover, the reproducibility of the proposed aptasensor was tested and low RSDs of 2.76, 4.57 and 2.50% were obtained.

MOFs-based aptasensors not only detect biomolecules, but also metal ions. In 2017, Xu et al. designed a label-free and enzyme-free electrochemical aptasensor for lead ion (Pb^{2+}) detection by linking the G-rich lead-specific aptamer (LSA) linked on the electrode (Xu et al., 2017). They used MIL-101(Fe) embedded with AgPt nanoparticles (AgPtNPs) as signal tags and sensitivity enhancer to amplify signals. Folded G-quadruplex structure was formed in the presence of Pb^{2+}; the remaining unfolded LSA would partially complement ssDNA (CS) to ensure CS-immobilized AgPtNPs/MIL-101(Fe) close to the electrode surface to provide detection signals. The aptasensor exhibited a LOD at 0.032 pM and the wider linearity from 0.1 pM to 100 nM. Liu et al. used Fe (III)-based metal-organic framework (Fe-MOF) and mesoporous Fe_3O_4@C nanocapsules (denoted as Fe-MOF@mFe_3O_4@mC) for heavy metal ion (Pb^{2+} and As^{3+}) detection utilizing the intrinsic properties such as high specific area, water stability and brilliant electrochemical activities (Zhang et al., 2017a) (Fig. 5b). The developed aptasensor exhibited a broad range from 0.01 to 10.0 nM for the detection of heavy metal ions. The LODs were 2.27 and 6.73 pM for Pb^{2+} and As^{3+}, respectively. Zn^{2+}, Ag^{+}, Ni^{2+}, Mg^{2+}, Ca^{2+}, Cu^{2+} and Mn^{2+} were used to determine the specificity of the biosensor. The negligible response (ΔRct values) showed excellent selectivity. Five isolated biosensors for the detection of Pb^{2+} and As^{3+} were used to obtain reproducibility. The RSDs of ΔRct values were 5.61% and 4.66%. Accurate detection of Pb^{2+} and As^{3+} was achieved when measuring river water and human blood serum samples. Both aforementioned aptasensors used specific aptamers and the formation of the G-quadruplex between metal ions and aptamers.

As can be seen above, MOFs-based electrochemical aptasensors are popular. Table 2 summarizes recent MOFs-based electrochemical aptasensors and their applications.

3.3. MOFs-based photoelectrochemical aptasensors

Diverse photoactive nanoparticles have photoelectrochemical (PEC) features such as CdS (Pardo-Yissar et al., 2003), TiO_2 (Tu et al., 2010), and ZnO (Kang et al., 2015). Using the PEC technology in biosensing has advantages of high sensitivity and selectivity owing to diverse characters of stimulus signals and response signals (Li et al., 2012b). Many MOFs' characteristics are beneficial for the enhancement of PEC properties of CdS by utilizing a wider spectrum for light-harvesting, and reducing charge carrier recombination. In a study conducted by Zhang et al. a photoelectrochemical aptasensor for the detection of AMP was constructed using CdS nanoparticles and europium metal-organic framework (Eu-MOF) (CdS/Eu-MOF). They discovered that the CdS/Eu-MOF modified electrode photocurrent was 2.5-fold stronger than that of the CdS modified electrode. Under optimum conditions, the

Table 2
MOFs-based electrochemical aptasensors by using MOFs as signal probes.

Type of MOFs	Target	Functionalization methods	Linear range	Detection limit	Ref
Tb-MOF-on-Fe-MOF	CA125	Hydrogen bond and covalent interaction	100 μU/mL - 200 U/mL	58 μU/mL	[(Wang et al., 2019c)]
Cu-MOF	Aβ	Au–S bond	1 nM - 2 mM	0.45 nM	[(Zhou et al., 2018)]
Cu-MOF	LPS		1.0 pg/mL - 1.0 ng/mL	0.29 pg/mL	[(Duan et al., 2020)]
ZnZr MOFs	PTK7	π−π stacking, hydrogen bonding, and Electrostatic interaction	1.0 pg/mL - 1.0 ng/mL	0.66 pg/mL	[(Zhou et al., 2019a)]
ZnNi MOF (1:2)	AD	Adsorption interaction	0.0001–100 ng/mL	20.32 fg/mL	[(Tian et al., 2020)]
Ce/Cu-MOF	TOB	Covalent interaction	0.01 pg/mL - 10 ng/mL	2.0 fg/mL	[(Wang et al., 2019d)]
Co-MOF	AMP	π–π stacking and hydrogen bond	1.0 fg/mL - 2.0 ng/mL	0.217 fg/mL	[(Liu et al., 2019b)]
Ce-MOF	OTC	π–π stacking and hydrogen bond	0.1–0.5 ng/mL	17.4 fg/mL	[(Zhou et al., 2019b)]
CuMOF	acetamiprid	Au–S bond	0.1 pM - 10.0 nM	2.9 fM	[(Qiao et al., 2019)]
Ni-MOF	thrombin	Au–NH_2 bond	0.05 pM - 50 nM	0.016 pM	[(Wu et al., 2019a)]
Co-MOF	ZEN	Pt–N or Pt–S bonds		1.37 fg/mL	[(He and Yan, 2020)]
MIL-101(Fe)	AFM1	Pt–N bond	0.01–80.0 ng/mL	2.0×10^{-3} ng/mL	[(Jahangiri-Dehaghani et al., 2020)]
Co-MOFs	thrombin	Pt–S bond	1 pM - 30 nM	0.32 pM	[(Yang et al., 2017a)]
Cu-MOF	MUC1	Amidation reaction	0.1 pM - 10 nM	0.033 pM	[(Hatami et al., 2019)]
ZIF-8	MC-LR	Au–S bond	0.01–50 ng/mL	0.006 ng/mL	[(Wu et al., 2020b)]
ZrHf-MOF	HER2 and MCF-7 cells	Electrostatic interaction	0.001–10 ng/mL; 1×10^2–1×10^5 cell/mL	19 fg/mL; 23 cell/mL	[(Gu et al., 2019)]
MIL-101(Fe)	Pb^{2+}		0.1 pM - 100 nM	0.032 pM	[(Xu et al., 2017)]
Fe-MOF	Pb^{2+} and As^{3+}	Supramolecular stacking and hydrogen bond	0.01–10.0 nM	2.27 and 6.73 pM	[(Zhang et al., 2017a)]
Fe-MOF	OTC	Amidation interaction	0.005–1.0 ng/mL	0.027 pg/mL	[(Song et al., 2017)]
UiO-66-2NH_2	MCF-7 cells	Zr–O–P bond	100 - 100,000 cell/mL	31 cell/mL	[(Li et al., 2020)]
Cu-MOFs	LPS	Electrostatic interaction	1.0 fg/mL - 100 ng/mL	0.33 fg/mL	[(Shen et al., 2015)]

biosensor exhibited a wide linear range from 1×10^{-10} to 2×10^{-7} M with the LOD of 9.3×10^{-11} M. This aptasensor was successfully applied to the detection of AMP in lake water and milk samples (Gao et al., 2019). Zhang et al. fabricated a label-free PEC sensor to detect tetracycline (Tc) by utilizing MIL-68(In)–NH_2/MWCNT/CdS as an efficient transducer (Zhang et al., 2019a). The MIL-68(In)–NH_2/MWCNT/CdS composites were prepared through the solvothermal method, and were dropped on the surface of an electrode. Then, the Tc-binding aptamer was immobilized on the surface of the composites-modified electrode to capture Tc molecules in solution. When Tc molecules were present, they would bind to the modified electrode, resulting in an increasing photocurrent signal via an instantaneous reaction between trapped Tc molecules and photo-generated holes. Owing to the ability of accelerating charge transfer and inhibiting the recombination of charge carriers, MIL-68(In)–NH_2/CdS served as ideal nanomaterials for PEC aptasensor. The certain aptasensor displayed a low LOD of 0.015 nM with a wide linear range of 0.1 nM–1 μM. Interferents including chloramphenicol, ciprofloxacin and diclofenac were chosen to explore the selectivity. The negligible photocurrent change was obtained (Fig. 5c). In addition to speeding up electron transfer, using MOFs as an obstructer of electrons is another approach for detection applications. Lu et al. introduced Ag/ZnMOF in a PEC aptasensor (Kong et al., 2020). In their report, Ag/Zn-MOF was chosen because of its steric hindrance effect and the peroxidase-mimicking property. Both properties resulted in impeding electron transfer and reducing photocurrent. Upon the addition of the target bleomycin (BLM), the signal was recovered. The proposed aptasensor was used to sensitively detect BLM at a low concentration of 0.18 nM with a linear range of 0.5 nM–500 nM.

Almost all kinds of MOFs in this field provide a synergistic effect to QDs by accelerating electron transfer, thereby enhancing photocurrent intensity. MOFs-based PEC aptasensor has inevitable drawbacks of high cost and sophisticated instruments and operation owing to the combination of light and electric signals. However, the merits would promote further development of PEC aptasensors.

4. MOFs as nanocarriers for aptamer-based biosensing

The large specific area and porous structure are the salient features of MOFs, which provide more interfaces and active sites for the interactions between materials and analytes. Meanwhile, the rich groups of organic ligands provide MOFs ease of functionalization with various molecules and materials. These characteristics make MOFs ideal carriers for loading signal probes to fabricate biosensors. MOFs act as nanocarriers to load signal molecules to promote signals owing to large specific areas and stable structures. In this section, we will introduce recent biosensors in which MOFs act as nanocarriers to load small molecules, enzymes, and other nanomaterials. Table 3 lists these different aptasensors using MOFs as nanocarriers to load various materials for the purpose of biosensing.

4.1. MOFs as small signal molecule carriers

In these types of aptasensors, small signal molecules such as methylene blue (MB), ferrocene (Fc), and some fluorescence signal substances are often used. He et al. explained an interesting aptasensor using MOFs for the detection of patulin (PAT) (He and Dong, 2019). The MOF@MB@aptamer served as signal tags owing to the hierarchically porous structure of MOFs. The MOFs (UIO-66-NH_2) were prepared and used as carriers for the adsorption and immobilization of MB. The resulting conjugates were functionalized with GA for the covalent linking of an amino-functionalized aptamer to obtain MOF@MB@aptamer. Then, the MOF@MB@aptamer signal tags were immobilized on the electrode with the complementary ssDNA to generate electrochemical signals. In the presence of PAT, PAT combined with the aptamer and took away the signal tags from the electrode, causing signal decrease (Fig. 6a). The results indicated that the aptasensor had a wide linear range from 5×10^{-8} to 5×10^{-1} μg/mL and the LOD of 1.46×10^{-8} μg/mL PAT. Its practical application potential was verified by detecting PAT in apple juice with a standard addition method. Similarly, a signal-off electrochemical aptasensor for the measurement of Ochratoxin A (OTA) was reported by using Zr MOFs (UIO-66) as the signal molecule carrier. The Zr in MOFs could bind the phosphate group (-PO_4^{3-}) on the end of the aptamer to form aptamer-MOFs through the specific coordination between Zr^{4+} and -PO_4^{3-}. Meanwhile, through the same coordination interaction, the MOFs could adsorb the MB-DNA-PO_4^{3-} to form aptamer-MOFs-MB, which was used as the signal probe. When testing OTA, it combined with the aptamer and took away the aptamer-MOFs-MB from electrodes. The higher OTA concentration, the

Table 3
Typical aptasensors by using MOFs as nanocarriers.

Type of MOFs	Loaded materials	Target	Functionalization methods	Linear range	Detection limit	Ref
Cu-MOF	PANI	*E. coli* O157: H7	Covalent interaction	2.1×10^{1}–2.1×10^{7} CFU/mL	2 CFU/mL	[(Shahrokhian et al., 2018)]
UiO-66-NH_2	MB	PAT	Covalent interaction	5×10^{-8}–5×10^{-1} μg/mL	1.46×10^{-8} μg/mL	[(He and Dong, 2019)]
UiO-66-NH_2	MB	CEA	Amidation interaction	50 fg/mL - 10 ng/mL	16 fg/mL	[(Bao et al., 2020)]
ZIF-8	Fc	*P. aeruginosa*	Amidation interaction	1.2×10^{1}–1.2×10^{7} CFU/mL		[(Shahrokhian et al., 2019)]
Fe-MOF	PEI	MPT64	Au–S bond	1 fg/mL - 1 ng/mL	0.33 fg/mL	[(Chen et al., 2019)]
Fe-MIL-88	Pt, DNAzyme	CAP	Pt–S bond	0.1 pM–1000 pM	0.03 pM	[(Luan et al., 2018)]
Zr-MOF	Pb^{2+}, Cd^{2+}	CAP and OTC	Amine-glutaraldehyde reaction		33 and 48 fM	[(Chen et al., 2017)]
Ce-MOFs	AuNPs	LPS	Au–S bond	10 fg/mL - 100 ng/mL	3.3 fg/mL	[(Shen et al., 2016)]
ZIF-8	Au	thrombin	Electrostatic interaction	0.1 pM - 20 nM	15 fM	[(Zhang et al., 2019b)]
Co-MOFs	PtNPs	thrombin	Pt–N bond	0.1 pM - 50 nM	0.33 fM	[(Yang et al., 2017b)]
521-MOF	AuNCs	cocaine	Zr–O–P bond	0.001–1.0 ng/mL	1.29 pM	[(Su et al., 2017)]
Ce-MOF	AuPtRu	TSP-1	Au–NH_2 bond	1 fg/mL - 10 ng/mL	0.13 fg/mL	[(Fu et al., 2019a)]

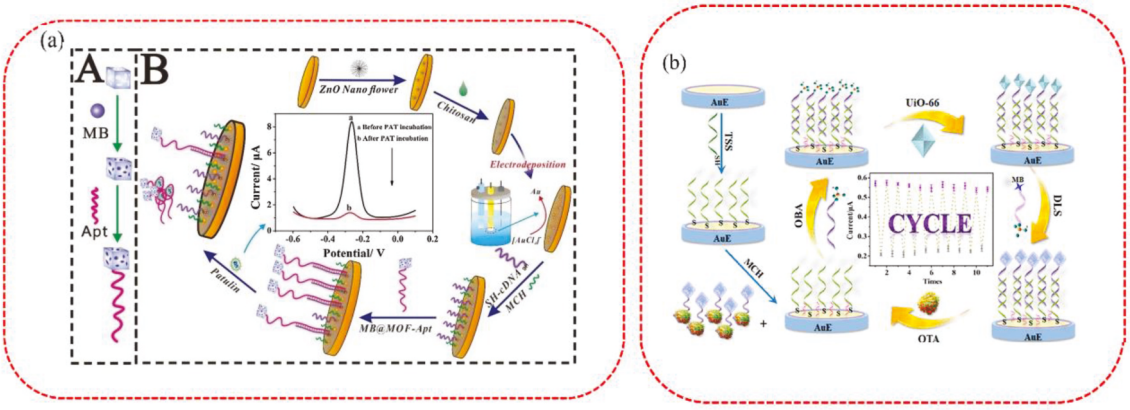

Fig. 6. Aptasensors using MOFs as small signal molecule nanocarriers. (a) A signal-off electrochemical aptasensor based on UIO-66-NH_2 decorated with MB as signal tags and C60NPs N-CNTs/GO nanocomposite. Reproduced with permission from (He and Dong, 2019). (b) A signal-off detection process using an electrochemical strategy based on Zr-MOFs and MB@Phosphate-terminated DNA. Reproduced with permission from (Qiu et al., 2020).

more current decrease was shown. The developed aptasensor showed a wide detection linear range from 0.1 fM to 2.0 μM and an ultralow LOD of 0.079 fM (Qiu et al., 2020) (Fig. 6b). Shahrokhian et al. proposed an electrochemical aptasensor based on zeolitic imidazolate Framework-8 (ZIF-8) via the EDC-NHS (EDC, 1-ethyl-3-(3-dimethylaminopropyl)carbodiimide; NHS, N-hydroxysuccinimide) strategy to link aptamers for the detection of *Pseudomonas aeruginosa* (*P. aeruginosa*). In this report, they introduced Fc-GO as an electroactive indicator and monitored resistance changes during the connection and the departure of Fc-GO with Apt/ZIF-8/GCE. The biosensor exhibited a wide linear range of 1.2×10^{1}–1.2×10^{7} and the LOD of 1.0 CFU/mL (Shahrokhian et al., 2019).

4.2. MOFs as enzyme carriers

Enzyme is a type of protein or RNA originated from living cells with high specificity and high catalytic efficiency, which is characterized by the integrity of the molecule's spatial structure and primary structure. Due to its catalytic activity, an enzyme can be used to catalyze the substrate and generate signals for detection in biosensors. However, the natural enzyme is susceptible to environmental influences, and the loss of catalytic activity occurs once the enzyme is denatured or subunits are depolymerized. Immobilization of the enzyme is an effective way to maintain the enzyme activity. MOFs are excellent carriers for immobilization of enzymes, and their outstanding biocompatibility promotes the conjugation between MOFs and enzymes, resulting in the combination of strengths of these two in the field of biosensing. A great deal of work on the immobilization of enzymes on MOFs has been reported, and some of these complexes have been used in aptasensors. Xie et al. fabricated an aptasensor for thrombin biosensing by using Fe-MIL-88 MOF as a carrier for loading hemin and glucose oxidase (GOD) (Xie et al., 2015). When the target thrombin existed, the sandwich structure formed. The GOD could oxidize glucose into gluconic acid accompanied by the generation of H_2O_2. The generated H_2O_2 on the electrode surface was further electrocatalyzed by hemin@MOFs to amplify the electrochemical signal. With such an ingenious design, a wide linear range of 0.0001 nM–30 nM was acquired with a relatively low LOD of 0.068 pM for thrombin detection. This sensitivity is comparable with the previous work (LOD of 0.016 pM) (Wu et al., 2019a). Similarly, Chen et al. used MOFs UIO-66 as a carrier for loading HRP and G-quadruplex/hemin (GQH) DNAzyme. The as-prepared composite used as the signal probe was functionalized with the cardiac troponin I (cTnI) aptamer for target recognition. In the presence of cTnI, an aptamer-protein-nanoprobe sandwich-type structure was formed. Afterward, the composite catalyzed the oxidation of hydroquinone by hydrogen peroxide for the electrochemical detection at a working potential of −0.1 V (vs. Ag/AgCl). The voltammetric signal increased linearly in the concentration range between 0.01 and 100 ng/mL cTnI, and the LOD was 5.7 pg/mL (Luo et al., 2019).

Enzymes are also loaded in MOFs for electrochemical impedimetric signals. Xu et al. reported an aptasensor for the detection of CEA. A series of redox reactions were used to finally generate non-conductive insoluble precipitates (IPs), which increased impedance signals (Zhou et al., 2017). In their report, Cu-MOFs were used as a carrier for the immobilization of GOD and hemin to form GOD-hemin@Cu-MOFs as the signal probe. The presence of CEA led to the formation of a sandwich structure and brought in the signal probe. When 3,3-diaminobenzidine (DAB) and glucose were introduced, a cascade reaction was initiated by GOD's catalyzing the oxidation of glucose, *in situ* generating H_2O_2. Then, hemin@Cu-MOFs with the peroxidase-like activity catalyzed the

decomposition of H_2O_2, accompanied with the oxidation of DAB and the formation of IPs, which led to enhanced electrochemical impedimetric signals. The aptasensor showed high sensitivity for CEA with the LOD of 0.023 pg/mL and a linear range from 0.05 pg/mL to 20 ng/mL. Moreover, the aptasensor showed good reproducibility, as manifested by the RSD of 1.3% for intra-batch measurement and 3.1% for inter-batch (Fig. 7).

4.3. MOFs as metal nanoparticle carriers

Owing to the important role of intrinsic catalysis, biocompatibility, electrochemical or optical activity, metal nanoparticles have attracted tremendous attention in recent years regarding detection applications. Some particles, such as silver and gold nanoparticles, can facilely enter into the tunnels or be adsorbed onto the surface of MOFs through self-assembly, leading to simpler operation processes and higher detection performance. Zhang et al. reported an electrochemical and surface plasmon resonance spectroscopy (SPR) aptasensor for the detection of CEA based on silver nanoclusters (Ag NCs) anchored Zr-MOF (UIO-66) with the CEA-targeted aptamer (Guo et al., 2017) (Fig. 8a). As an ideal carrier, Zr-MOF with high specific surface area loaded a great amount of Ag NCs, which were used as signal probes with high electrochemical activity, strong SPR response, and acceptable fluorescence performance. The CEA-targeted aptamer was first used as the template to adsorb Ag^+ and synthesize the Ag NCs@Apt, which was further embedded in the UiO-66 frameworks. In the presence of CEA, the aptamer specifically bound to CEA, which resulted in considerably low access of the redox probe (K_3 [$Fe(CN)_6$]/K_4 [$Fe(CN)_6$]) to the surface of Ag NCs@Apt@UiO-66 frameworks and the decrease in electrochemical response. Meanwhile, the binding between CEA and the aptamer layer induced changes in the dielectric constant of the thin adjacent layer and its thickness, thereby leading to the variation in the corresponding resonance reflectivity of SPR. Therefore, the AgNC@Apt@UIO-66 could be used to fabricate electrochemical and SPR aptasensors simultaneously. Both the electrochemical and SPR aptasensors exhibited high sensitivity and selectivity. The electrochemical aptasensor showed a low LOD of 8.88 and 4.93 pg/mL by using EIS and DPV, respectively, within a broad linear range of the CEA concentration (0.0–10 ng/mL). Meanwhile, the SPR biosensor based on AgNC@Apt@UIO-66 showed a LOD of 0.3 ng/mL with a CEA linear concentration range from 1.0 to 250 ng/mL. Different kinds of interfering agents (ascorbic acid (AA), mucin 1 (MUC1), thrombin, and immunoglobulin G (IgG)) were tested with no interfering effects on CEA detection. The research could promote the potential application of metal nanoparticle/MOFs composites in clinical diagnosis. Zhang et al. introduced Au nanoparticle@ZIF-8(NiPd) as a signal probe and promising nanocarriers for biomarker detection. Au@ZIF-8(NiPd) plays the role of peroxidase mimics for catalyzing H_2O_2 reduction (Zhang et al., 2019b) (Fig. 8b). The proposed aptasensor exhibited a linear range of 0.1 pM–20 nM with a LOD of 15 fM. For the specificity investigation, the interferents had similar signal responses compared to blank samples. The reproducibility was evaluated using five aptasensors and the RSD was 4.96%. After 10 days, only 86.6% of the initial signal remained. Yuan's group developed an electrochemical aptasensor using Pt nanoparticles-functionalized Co-MOFs (PtNPs@Co-MOFs@PtNPs) to detect thrombin (Yang et al., 2017b). Owing to the electron transfer activity from Co^{2+} to Co^{3+}, PtNPs@Co-MOFs@PtNPs was used as the redox media to generate charge and transfer electrons. With the additional catalysis of PtNPs to H_2O_2, this aptasensor had a LOD of 0.33 fM and a wide linear range of 0.1 pM–50 nM. A sensitive electrochemical aptasensor to detect lipopolysaccharide (LPS) with the assistance of Ce-MOF decorated with AuNPs was also reported. The AuNPs/Ce-MOFs was applied as a catalyst for AA oxidation to generate

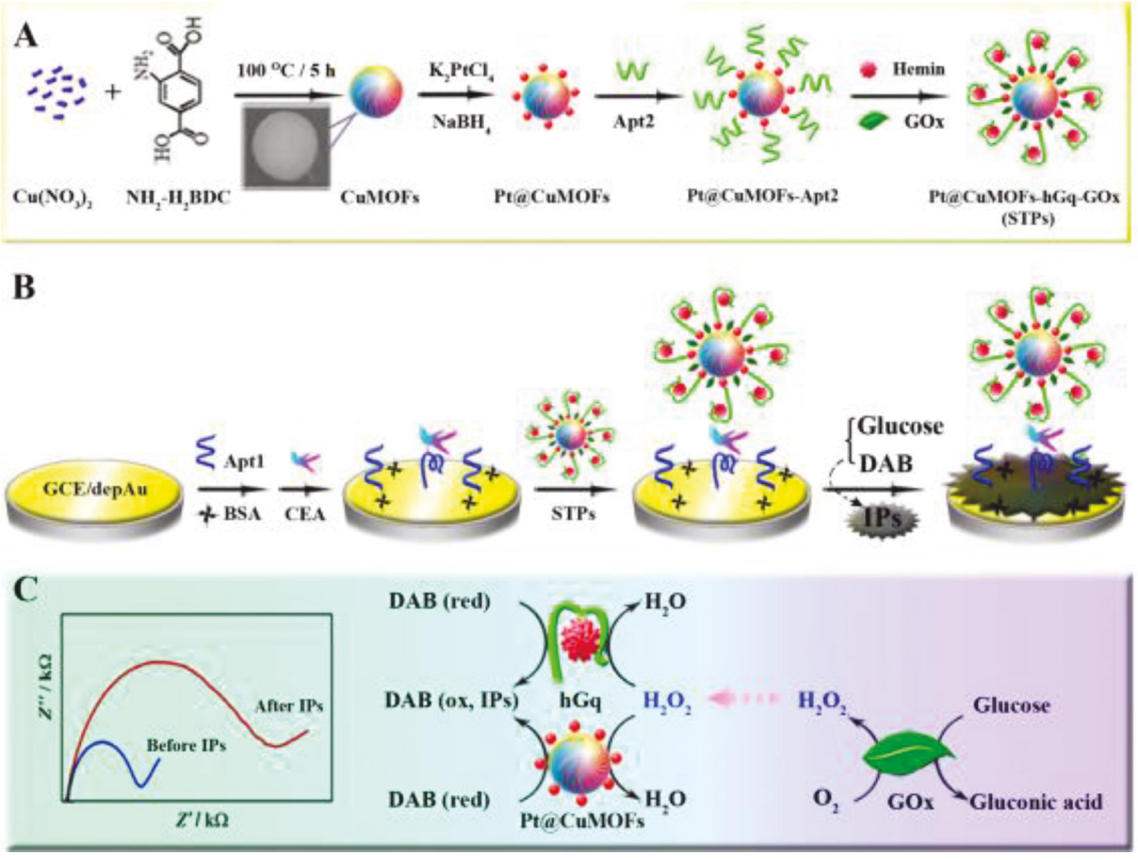

Fig. 7. Aptasensors using MOFs as nanocarriers for loading enzyme. An impedimetric aptasensor based on Cu-MOFs decorated with GOD and hemin as signal probe. Reproduced with permission from (Zhou et al., 2017).

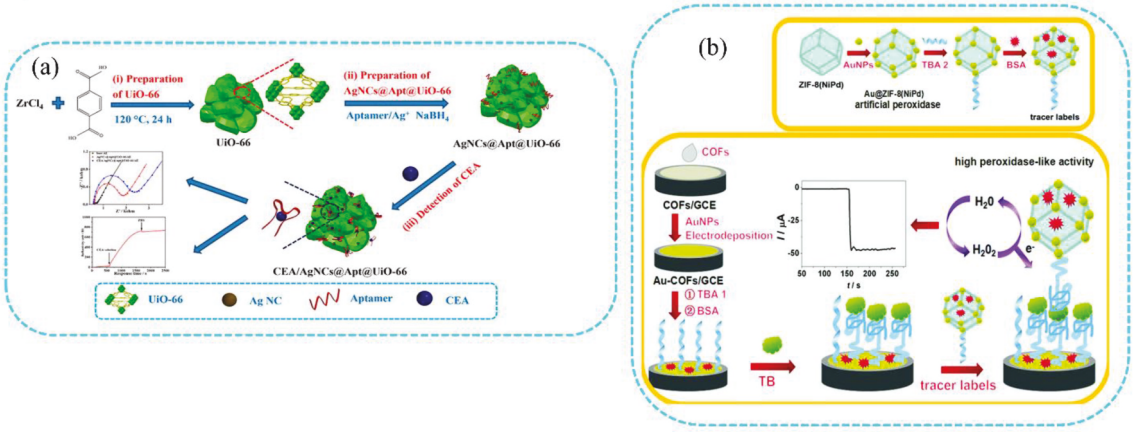

Fig. 8. Aptasensors using MOFs as nanocarriers to load metal nanoparticles. (a) UIO-66 embedded silver clusters were used as aptasensors for the detection of CEA. Reproduced with permission from (Guo et al., 2017). (b) A sandwich electrochemical aptasensor based on Au-COFs and Au@ZIF-8(NiPd). Reproduced with permission from (Zhang et al., 2019b).

signals (Shen et al., 2016). Under the optimized conditions, this proposed aptasensor for LPS exhibited a low LOD of 3.3 fg/mL with a wide linear range from 10 fg/mL to 100 ng/mL. Su et al. prepared a 2D Zn-MOF nanosheet conjugated with Au nanoclusters (2D AuNCs@521-MOF), which had excellent bioaffinity towards biomolecule-bearing phosphate groups and good electrochemical activity from AuNC. It was used to detect cocaine due to the specific binding interactions between aptamers on the MOFs and cocaine (Su et al., 2017).

MOFs with metal nanoparticles immobilized on an electrode surface also become modified materials. After modification, they demonstrate large specific surface areas, excellent electronic transmission capability, strong adsorption capacity, and good biocompatibility, which are beneficial to electrochemical signal amplification. Yu et al. used Ce-MOF@Au as electrode modification materials and trimetallic AuPtRu NPs as signal tags to construct an electrochemical aptasensor for thrombospondin-1 (TSP-1) detection (Fu et al., 2019a). AuPtRu NPs served as the catalyst to catalyze H_2O_2 for signal transduction. By using Ce-MOF@AuPtRu composites for signal amplification, the aptasensor showed excellent sensitivity for the detection of TSP-1. The proposed aptasensor exhibited a low LOD of 0.13 fg/mL in a linear range of 1 fg/mL to 10 ng/mL. This approach was expected to have potential for the auxiliary diagnosis of various diseases caused by TSP-1. In the same manner, Bai et al. used polyethyleneimine (PEI)-functionalized Fe-based MOFs (P-MOFs) as electrode-modified materials to speed up the electron transfer (Chen et al., 2019). C_{60}NPs-N-CNTs/GO bound to aptamer II (MAA II) acted as a signal probe and was beneficial for the signal amplification. The electrochemical aptasensor showed a wide dynamic range from 1 fg/mL to 1 ng/mL with a LOD of 0.33 fg/mL for MPT64 antigen (*Mycobacterium tuberculosis* antigen) detection.

5. Stimuli-responsive aptamer-functionalized MOFs

Stimuli-responsive porous materials, featured with high surface areas and unique pore structures, have attracted substantial research interests (Balogh et al., 2015). Mesoporous silica is the most extensively explored porous material owing to its large loading capacity, adjustable pore size, nontoxic nature, biocompatibility, and ease of functionalization (Cheng et al., 2018, 2019). However, the small pore volume and irregular pore size limit the application of mesoporous silica as a nanocontainer. Instead, as a kind of porous materials, MOFs have an excellent ability for encapsulation of guest molecules in pores and controllable releasing of guest molecules by smart gatekeepers. More importantly, MOFs have a more regular pore structure and exact nucleic acid functionalization sites for encapsulation. Therefore, nucleic acid-functionalized MOFs have attracted substantial attention to the fabrication of stimuli-responsive devices (Simon-Yarza et al., 2018; Hidalgo et al., 2020). Willner group is one of the earliest research groups to use nucleic acid-functionalized MOFs to fabricate stimuli-responsive nanocontainers, which can be used for drug delivery and ion sensing (Kahn et al., 2017; Zhou et al., 2017). First, the amine-modified DNA reacted with dibenzocyclooctyne-sulfo-N-hydroxysuccinimidyl ester (DBCOsulfo-NHS ester) to form DBCO-modified DNA. Then, the DBCO-modified DNA bound to azide groups conjugated onto MOFs. Finally, the other oligonucleotide hybridized with DNA on MOFs by complementary base pairing to form intact capping units. In the regulation of pH, the drug would be released and have selective cytotoxicity for certain cells. With the inspiration, new biosensing methods based on the bio-molecular-gated release strategy and stimuli-responsive MOFs have been developed. The signal transduction and amplification can be realized easily by the bio-gated and stimuli-responsive release of a large number of signal molecules from MOFs, such as rhodamine, MB, Thi, and Fc. Li's group adopted MOFs to fabricate a homogeneous electrochemical biosensor for the simultaneous detection of multiple tumor biomarkers (Chang et al., 2019). In this research, UIO-66-NH_2 was used as a nanocontainer to load two kinds of electroactive dyes (MB and TMB) by using two kinds of double-stranded DNA as the gatekeeper to cap MOFs, respectively. The recognition and hybridization of nucleic acids with target miRNAs (let-7a and miRNA-21) impelled the generation of RNA-DNA complexes. Hence, the double-stranded DNA dissociated, allowing MB and TMB to be released. For the simultaneous detection of two biomarkers (let-7a and miRNA-21), MB and TMB corresponded to different double-stranded DNAs and target miRNAs. Thus, simultaneous detection of let-7a and miRNA-21 was achieved, with the LODs down to 3.6 and 8.2 fM, respectively (Fig. 9a). Interestingly, it used two electroactive elements to realize simultaneous electrochemical detection. In a similar strategy, Wang et al. designed a DNA-gated-MOFs biosensor based on target-driven MB release processes (Bao et al., 2020). In the presence of the target, the nicking endonuclease cleavage process was triggered, resulting in the generation of two strands (S1 and S2). The generated S1 and S2 acted as stimuli to participate in the strand displacement reaction on the MB@DNA/MOFs, which unlocked the pore to release MB, leading to the decrease of electrochemical signals. Through two amplification cycles, the electrochemical performance was significantly improved, with the LOD of 16 fg/mL for CEA with DPV.

To improve the biocompatibility and ease of operation, the MOFs-derived porous carbon has been used for the fabrication of stimuli-responsive aptasensors. We proposed a simple homogeneous electrochemical stimuli-responsive aptasensor for thrombin sensing by combining aptamer bio-gate with ZIF-8-derived porous carbon

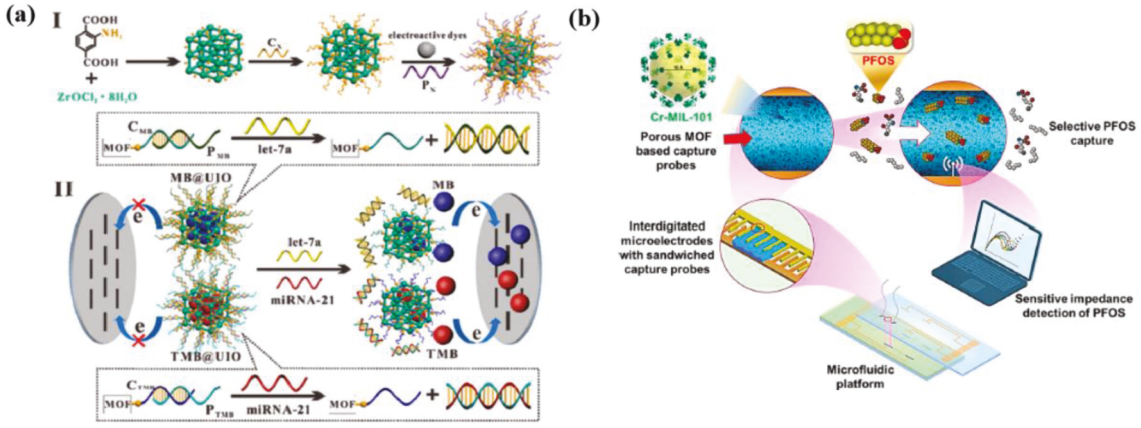

Fig. 9. (a) Stimuli-responsive sensors using nucleic acid-functionalized MOFs as nanocarriers to encapsulate drug/signal probes. A homogeneous electrochemical biosensor with MB and TMB encapsulated in nucleic acid-functionalized UIO-66 was assembled for simultaneous detection of two tumor biomarkers. Reproduced with permission from (Chang et al., 2019). (b) Integration of MOFs-based sensors in a microfluidic platform for rapid and *in situ* molecular detection. Ultrasensitive *in situ* detection of perfluorooctanesulfonate (PFOS) was achieved by a MOF-based (Cr-MIL-101) impedance sensor integrated in a microfluidic platform. Reproduced with permission from (Cheng et al., 2020).

nanocontainers (Ren et al., 2020). The porous carbon nanocontainer (Z-700) was synthesized by direct carbonization of ZIF-8. MB was loaded into the pores of Z-700 as a signal probe, while the pores were capped with the thrombin-binding aptamer through the π-stacking interaction between the nucleobases and carbon nanostructure. In the presence of the target, the thrombin-binding aptamer detached from the Z-700 surface, and the aptamer molecular gate was opened, leading to the release of MB. The released MB could be quantitatively monitored by a screen-printed electrode without sample separation and washing procedures. The proposed strategy demonstrated satisfactory performances for the detection of thrombin (with a wide detection range from 1 fM to 1 nM and a low LOD of 0.57 fM) and could be conveniently extended to a wide range of other analytes. The reproducibility of the aptasensor was evaluated and the RSD 2.3% was achieved. In addition, using spiked human serum samples, the measured recoveries were 95.65%–98.32% with the RSDs ranging from 5.32% to 7.45%.

6. Integration of MOFs on microfluidic devices

Despite the significant progress in the synthesis and application of various types of MOFs in recent years, the control of their shapes and sizes remains a challenge, particularly in environmentally friendly syntheses. Furthermore, the developed MOFs-biosensors often lack portability, integration, ease of operation, rapid assays, and high throughput, limiting their wide application in biosensing, POC detection, and environmental surveillance. Microfluidic technology developed during the 1990s, also called lab-on-a-chip (LOC), a type of miniaturized devices mostly produced by the microfabrication technique, has developed rapidly in the last few decades (Li et al., 2012c, 2013). It has emerged as a versatile platform for various biomedical, environmental, and other applications (Dou et al., 2014; Dou et al., 2015; Dou et al., 2016a; Dou et al., 2016b; Dou et al., 2017a; Dou et al., 2017b; Dou et al., 2019a; Dou et al., 2019b; Fu et al., 2019b; Fu et al., 2019c; Fu et al., 2020; Liu et al., 2011a; Liu et al., 2011b; Prasad et al., 2020a; Prasad et al., 2020b; Sanjay et al., 2015; Sanjay et al., 2016b; Sanjay et al., 2018; Shen et al., 2014; Shen et al., 2017; Tavakoliet al., 2019b; Tavakoli et al., 2020; Wei et al., 2018; Xu et al., 2019; Zhang et al., 2017b; Zhou et al., 2020c). It allows for low reagent consumption, fast analysis, high portability, and integrated processing and analysis of complex biological fluids with high efficiency and sensitivity as well as the opportunity for rapid and multiplexed detection (Zuo et al., 2013; Dou et al., 2017b; Y. Zhou et al., 2020a; Dou et al., 2019b; Fu et al., 2019b; Fu et al., 2019b; Xu et al., 2019; Prasad et al., 2020). Given those advantages, microfluidic lab-on-a-chip provide a unique opportunity for MOFs in controlled synthesis and detection applications.

6.1. Controlled synthesis of MOFs in microfluidic devices

Because the microfluidics technology allows not only the continuous production of MOFs, but also the accurate control of reaction parameters in the synthesis processes, it provides an excellent platform for the controlled synthesis of MOFs. Many microfluidic approaches have been proposed for the controlled synthesis of MOFs beyond the conventional solvothermal technique, especially MOFs membranes and the MOFs composites (Echaide-Górriz et al., 2018). A metal-containing solution and an organic ligand solution are often introduced for the synthesis of MOFs using a microfluidic system through separate inlets/channels. Solutions then co-flow in one microfluidic channel in a laminar flow format or a droplet format (Paseta et al., 2013; Wu et al., 2019b; Wang et al., 2018b). Interfacial reactions play an essential role in the microfluidic synthesis of MOFs, as we reported previously in a microfluidic interfacial nano-biosensing study (Dou et al., 2016a). This technology has the advantages of high-throughput, high controllability, and ease of preparation. For instance, Brown et al. used a microfluidic approach to fabricate continuous molecular sieving ZIF-8 membranes in hollow fibers, which has excellent potential for energy-efficient chemical separations (Brown et al., 2014). Faustini et al. prepared many kinds of core-shell MOF composites by exploiting a unique two-step integrated microfluidic synthesis scheme in a continuous-flow mode (Ganiga and Cyriac, 2016). Since MOF synthesis is not the emphasis of this review, more work regarding this topic can be found from other articles (Echaide-Górriz et al., 2018; Brown et al., 2014; Wang et al., 2018b).

6.2. Introduction of MOFs into microfluidic devices for sensing

As mentioned earlier, although MOFs-based biosensors have numerous advantages, including large specific areas, porous structures, ease of functionalization, and high catalytic activities for developing high-performance sensors, they still have limitations in low portability, integration, complicated operation, lengthy assays, and low throughput, limiting their wide applications in POC detection, especially in low-resource settings. Interestingly, many MOF limitations are the advantages of microfluidic systems. The combination of MOFs-based biosensors on a microfluidic device can complement each component, providing tremendous potential for integrated high-performance molecular detection in various fields.

Researchers in recent years have endeavored to integrate MOFs on microfluidics to fabricate biosensors with advantages from both MOFs and microfluidics. MOFs can be embedded inside microfluidic channels. Due to the high surface area, high pore volume, abundant ingredients and groups, the MOFs-based microfluidic biosensor can achieve great analytical performance. In 2019, Chen's group introduced a microfluidic device integrated with a biosensor based on MOFs and enzymes (Mohammad et al., 2019). Biomineralization of enzymes in MOFs to improve enzyme stability and polydopamine/polyethyleneimine (PDA/PEI) coating to pattern enzyme/MOFs in microfluidic channels were employed to assemble biosensors in a polydimethysiloxane (PDMS)-based microfluidic device. They combined a cascade reaction of glucose oxidase (GOx) and HRP enzyme in a patterned ZIF-8 thin film to detect glucose. ZIF-8/GOx&HRP *in situ* exhibited high selectivity toward glucose, obtaining a LOD of 8 μM for glucose detection. Significantly, the team found the ability of the ZIF-8 thin-film structure to provide a diffusion-limiting effect for substrate influx in a microfluidic channel, achieving a wide linear range from 8 μM to 5 mM of glucose. A similar phenomenon for a wide linear range was also observed in our recent work in ultrasensitive on-chip immunoassays (Sanjay et al., 2020). Moreover, the combination of MOF-based biosensors with microfluidics enables rapid, sensitive, *in situ* detection of pollutants to improve public environmental safety. In 2020, Cheng et al. developed a MOF-based impedance sensor using a microfluidic platform for ultrasensitive *in situ* detection of perfluorooctanesulfonate (PFOS) (Cheng et al., 2020). This work demonstrated a synergistic approach for the targeted affinity-based capture of PFOS using a porous sorbent probe, which enhanced detection sensitivity by embedding the probe on a microfluidic platform. The mesoporous MOF Cr-MIL-101 with high surface areas and pore volumes was used as the probe for the targeted PFOS capture based on the affinity of the chromium center toward both fluorine tail groups as well as the sulfonate functionalities. The MOF capture probes were sandwiched between interdigitated microelectrodes in a microfluidic channel, forming an impedance sensor in a portable microfluidic device. This microfluidic platform integrated with a MOFs-based sensor exhibited ultrasensitivity for the rapid *in situ* detection of PFOS. The LOD was obtained as 0.5 ng/L, which was comparable to that of state-of-the-art ex situ techniques (Fig. 9b).

7. Conclusion and future perspectives

This article reviews recent advances of various aptamer-functionalized MOF-based sensors and their bio-applications. Due to the variable composition and groups of MOFs, aptamer can functionalize MOFs easily and stably with different methods for the target recognition. For signal transduction, MOFs act not only as signal probes directly, but also as carriers for loading signal probes. Due to remarkable advantages of MOFs and aptamers, numerous MOFs-based aptasensors have been developed and widely used in various applications with high sensitivity and high specificity. The integration of MOFs on microfluidic devices allows controlled synthesis of MOFs and high-performance biosensing on the GO.

However, MOFs-based aptasensors still face some challenges to overcome in order to obtain highly effective aptasensors. First, it is still challenging to control their shape and size, particularly in environmentally friendly syntheses, whereas the size, morphology, and structure of MOFs can significantly affect a sensor's performance. To obtain an aptasensor with great sensitivity and accuracy, synthesizing nanoscale MOFs with uniform structures to improve active areas of the sensing interface and promote the mass/electron transfer efficiency will be an effective method. MOF synthesis using microfluidic platforms may provide a superior solution to address these challenges. Second, the effective and precise immobilization of aptamers on specific sites of MOFs is a key factor for the reproducibility of biosensors. Therefore, the introduced decorated groups, the functionalization methods, and the ratio of aptamers per MOF may need to be systematically studied. To overcome this challenge, developing theoretical models by computational methods to analyze the functionalized aptamers amount can contribute to the improvement of functionalization efficiency, sensing accuracy and reproducibility. Third, not all targets have their corresponding aptamers available, and the availability of aptamers to different targets is still limited. Additionally, the specificity of aptamers in complex matrixes, such as whole blood, is not high at times and thus needs to be further improved. Moreover, MOFs-based biosensors are often not portable, inconvenient to operate, and not suitable for *in situ* and practical applications. The demand for portable devices is increasing in many fields, such as POC diagnostics, rapid on-site infectious disease screening, global health in developing nations, environmental surveillance, and food safety inspection. The integration of MOFs-based biosensors with the microfluidic technology provides a unique opportunity for the future development of portable devices to meet such demand and has great potential for wide applications, though such a combination is still at its early stage. Overall, with a promising future ahead, new significant advances in MOFs-based biosensors require close collaborations from multiple disciplines, such as material science and engineering, nanoscience and technology, microfluidics, analytical chemistry, biosensors, biology, and biomedical science and applications.

Author contribution

Mengzhen Lv: Writing – original draft, Writing – review & editing, did literature search, drafted and revised the manuscript, Wan Zhou: Writing – original draft, Writing – review & editing, did literature search, drafted and revised the manuscript, Hamed Tavakoli: Writing – original draft, Writing – review & editing, did literature search, drafted and revised the manuscript, Cynthia Bautista: Writing – review & editing, mainly contributed the revision, Jianfei Xia: Methodology, conceived the idea and designed the project plan and the paper structure, Zonghua Wang: Writing – review & editing, mainly contributed the revision, XiuJun Li: Methodology, conceived the idea and designed the project plan and the paper structure.

Declaration of competing interest

The authors declare that they have no known competing financial interests or personal relationships that could have appeared to influence the work reported in this paper.

Acknowledgments

We would like to acknowledge the financial support from the National Institute of Allergy and Infectious Disease of the NIH (R21AI107415), the U.S. NSF (IIP 1953841), NIH/NIGMS (RL5GM118969, TL4GM118971, and UL1GM118970), the University of Texas at El Paso (UTEP) for the IDR Program, the Philadelphia Foundation, and the Medical Center of the Americas Foundation. The financial support to our prior research from the National Institute of General Medical Sciences of the NIH (SC2GM105584), the NIH RCMI Pilot Grant, the U.S. NSF (DMR1205302), the University of Texas (UT) System for the STARS award, and the Multidisciplinary Research Award Program (MRAP) and the URI Program from UTEP is also greatly acknowledged. We also thank the Dr. Keelung Hong Research Fellowship for the support to WZ. The authors JX and ZW appreciate the financial support from the Key Research and Development Project of Shandong Province, China (2019GGX102083) and the Taishan Scholar Program of Shandong Province (No. ts201511027).

References

Altintas, C., Avci, G., Daglar, H., Nemati Vesali Azar, A., Velioglu, S., Erucar, I., Keskin, S., 2018. ACS Appl. Mater. Interfaces 10, 17257–17268.

Balogh, D., Garcia, M.A.A., Albada, H.B., Willner, I., 2015. Angew. Chem. Int. Ed. 54, 11652–11656.
Bao, T., Fu, R., Wen, W., Zhang, X., Wang, S., 2020. ACS Appl. Mater. Interfaces 12, 2087–2094.
Brown, A.J., Brunelli, N.A., Eum, K., Rashidi, F., Johnson, J.R., Koros, W.J., Jones, C.W., Nair, S., 2014. Science 345, 72–75.
Cao, Y., Wang, L., Shen, C., Wang, C., Hu, X., Wang, G., 2019. Sensor. Actuator. B Chem. 283, 487–494.
Cavka, J.H., Jakobsen, S., Olsbye, U., Guillou, N., Lamberti, C., Bordiga, S., Lillerud, K.P., 2008. J. Am. Chem. Soc. 130, 13850–13851.
Chae, H.K., Siberio-Pérez, D.Y., Kim, J., Go, Y.B., Eddaoudi, M., Matzger, A.J., O'Keeffe, M., Yaghi, O.M., 2004. Nature 427, 523–527.
Chang, J., Wang, X., Wang, J., Li, H., Li, F., 2019. Anal. Chem. 91, 3604–3610.
Chen, M., Gan, N., Li, T., Wang, Y., Xu, Q., Chen, Y., 2017. Anal. Chim. Acta 968, 30–39.
Chen, Y., Liu, X., Guo, S., Cao, J., Zhou, J., Zuo, J., Bai, L., 2019. Biomaterials 216, 119253.
Cheng, H., Li, W., Duan, S., Peng, J., Liu, J., Ma, W., Wang, H., He, X., Wang, K., 2019. Anal. Chem. 91, 10672–10678.
Cheng, H., Liu, J., Ma, W., Duan, S., Huang, J., He, X., Wang, K., 2018. Anal. Chem. 90, 12544–12552.
Cheng, Y.H., Barpaga, D., Soltis, J.A., Shutthanandan, V., Kargupta, R., Han, K.S., McGrail, B.P., Motkuri, R.K., Basuray, S., Chatterjee, S., 2020. ACS Appl. Mater. Interfaces 12, 10503–10514.
Chughtai, A.H., Ahmad, N., Younus, H.A., Laypkov, A., Verpoort, F., 2015. Chem. Soc. Rev. 44, 6804–6849.
Dou, M., Dominguez, D.C., Li, X., Sanchez, J., Scott, G., 2014. Anal. Chem. 86, 7978–7986.
Dou, M., García, J.M., Zhan, S., Li, X.J., 2016a. Chem. Commun. 52, 3470–3473.
Dou, M., Lopez, J., Rios, M., Garcia, O., Xiao, C., Eastman, M., Li, X., 2016b. Analyst 141, 3898–3903.
Dou, M., Sanchez, J., Tavakoli, H., Gonzalez, J.E., Sun, J., Dien Bard, J., Li, X.J., 2019a. Anal. Chim. Acta 1065, 71–78.
Dou, M., Macias, N., Shen, F., Dien Bard, J., Domínguez, D.C., Li, X., 2019b. EClinicalMedicine 8, 72–77.
Dou, M., Sanjay, S.T., Benhabib, M., Xu, F., Li, X.J., 2015. Talanta 145, 43–54.
Dou, M., Sanjay, S.T., Dominguez, D.C., Liu, P., Xu, F., Li, X.J., 2017a. Biosens. Bioelectron. 87, 865–873.
Dou, M., Sanjay, S.T., Dominguez, D.C., Zhan, S., Li, X., 2017b. Chem. Commun. 53, 10886–10889.
Drake, T., Ji, P., Lin, W., 2018. Acc. Chem. Res. 51, 2129–2138.
Duan, N., Wu, S., Dai, S., Gu, H., Hao, L., Ye, H., Wang, Z., 2016. Analyst 141, 3942–3961.
Duan, Y., Wang, N., Huang, Z., Dai, H., Xu, L., Sun, S., Ma, H., Lin, M., 2020. Mater. Sci. Eng. C 108, 110501.
Echaide-Górriz, C., Clément, C., Cacho-Bailo, F., Téllez, C., Coronas, J., 2018. J. Mater. Chem. 6, 5485–5506.
Eddaoudi, M., Kim, J., Rosi, N., Vodak, D., Wachter, J., O'Keeffe, M., Yaghi, O.M., 2002. Science 295, 469–472.
Espiritu, C.A.L., Justo, C.A.C., Rubio, M.J., Svobodova, M., Bashammakh, A.S., Alyoubi, A.O., Rivera, W.L., Rollon, A.P., O'Sullivan, C.K., 2018. ACS Infect. Dis. 4, 1306–1315.
Feng, D., Gu, Z.Y., Li, J.R., Jiang, H.L., Wei, Z., Zhou, H.C., 2012. Angew. Chem. Int. Ed. 51, 10307–10310.
Feng, Q.M., Shen, Y.Z., Li, M.X., Zhang, Z.L., Zhao, W., Xu, J.J., Chen, H.Y., 2016. Anal. Chem. 88, 937–944.
Férey, C., Mellot-Draznieks, C., Serre, C., Millange, F., Dutour, J., Surblé, S., Margiolaki, I., 2005. Science 309, 2040–2042.
Fonseca, T.H.S., Faria, A.R., Leite, H.M., da Silveira, J.A.G., Carneiro, C.M., Andrade, H. M., 2019. Vet. J. 253, 105387.
Fu, G., Fu, G., Zhou, W., Li, X., Li, X., Li, X., 2020. Lab Chip 20, 2218–2227.
Fu, G., Sanjay, S.T., Zhou, W., Brekken, R.A., Kirken, R.A., Li, X., 2018. Anal. Chem. 90, 5930–5937.
Fu, G., Zhu, Y., Wang, W., Zhou, M., Li, X.J., 2019b. ACS Sens. 4, 2481–2490.
Fu, G., Zhu, Y., Xu, K., Wang, W., Hou, R., Li, X., 2019c. Anal. Chem. 91, 13290–13296.
Fu, X., He, J., Zhang, C., Chen, J., Wen, Y., li, J., Mao, W., Zhong, H., Wu, J., Ji, X., Yu, C., 2019a. Biosens. Bioelectron. 132, 302–309.
Ganiga, M., Cyriac, J., 2016. Sensor. Actuator. B Chem. 225, 522–528.
Gao, J., Chen, Y., Ji, W., Gao, Z., Zhang, J., 2019. Analyst 144, 6617–6624.
Gao, P., Sun, X.Y., Liu, B., Lian, H.T., Liu, X.Q., Shen, J.S., 2018. J. Mater. Chem. C 6, 8105–8114.
Gu, C., Peng, Y., Li, J., Liu, C.S., Pang, H., 2020. Appl. Mater. Today 20, 100745.
Gu, C., Guo, C., Li, Z., Wang, M., Zhou, N., He, L., Zhang, Z., Du, M., 2019. Biosens. Bioelectron. 134, 8–15.
Guo, C., Su, F., Song, Y., Hu, B., Wang, M., He, L., Peng, D., Zhang, Z., 2017. ACS Appl. Mater. Interfaces 9, 41188–41199.
Hai, X.M., Li, N., Wang, K., Zhang, Z.Q., Zhang, J., Dang, F.Q., 2018. Anal. Chim. Acta 998, 60–66.
Han, R., Sun, Y., Lin, Y., Liu, H., Dai, Y., Zhu, X., Gao, D., Wang, X., Luo, C., 2020. New J. Chem. 44, 4099–4107.
Hatami, Z., Jalali, F., Amouzadeh Tabrizi, M., Shamsipur, M., 2019. Biosens. Bioelectron. 141, 111433.
He, B., Dong, X., 2019. Sensor. Actuator. B Chem. 294, 192–198.
He, B., Yan, X., 2020. Sensor. Actuator. B Chem. 306, 127558.
He, J., Li, G., Hu, Y., 2017. Microchim. Acta 184, 2365–2373.
Hidalgo, T., Alonso-Nocelo, M., Bouzo, B.L., Reimondez-Troitiño, S., Abuin-Redondo, C., De La Fuente, M., Horcajada, P., 2020. Nanoscale 12, 4839–4845.
Jahangiri-Dehaghani, F., Zare, H.R., Shekari, Z., 2020. Food Chem. 310, 125820.
Jarczewska, M., Górski, Ł., Malinowska, E., 2016. Anal. Methods 8, 3861–3877.
Kahn, J.S., Freage, L., Enkin, N., Garcia, M.A.A., Willner, I., 2017. Adv. Mater. 29, 1–6.
Kang, Y.S., Lu, Y., Chen, K., Zhao, Y., Wang, P., Sun, W.Y., 2019. Coord. Chem. Rev. 378, 262–280.
Kang, Z., Gu, Y., Yan, X., Bai, Z., Liu, Y., Liu, S., Zhang, Xiaohui, Zhang, Z., Zhang, Xueji, Zhang, Y., 2015. Biosens. Bioelectron. 64, 499–504.
Kholafazad Kordasht, H., Pazhuhi, M., Pashazadeh-Panahi, P., Hasanzadeh, M., shadjou, N., 2020. Trac. Trends Anal. Chem. 124, 115778.
Kong, W., Guo, X., Jing, M., Qu, F., Lu, L., 2020. Biosens. Bioelectron. 150, 111875.
Li, H.L., Eddaoudi, M.M., O'Keeffe, M., Yaghi, O.M., 1999. Nature 402, 276–279.
Li, J., Wang, Xiangxue, Zhao, G., Chen, C., Chai, Z., Alsaedi, A., Hayat, T., Wang, Xiangke, 2018. Chem. Soc. Rev. 47, 2322–2356.
Li, Q., Zheng, J.Y., Yan, Y., Zhao, Y.S., Yao, J., 2012a. Adv. Mater. 24, 4745–4749.
Li, S., Yue, S., Yu, C., Chen, Y., Yuan, D., Yu, Q., 2019. Analyst 144, 649–655.
Li, X.J., Valadez, A.V., Zuo, P., Nie, Z., 2012c. Bioanalysis 4, 1509–1525.
Li, X.J., Zhou, Y., 2013. Microfluidic Devices for Biomedical Applications. Woodhead Publishing.
Li, Y., Hu, M., Huang, X., Wang, M., He, L., Song, Y., Jia, Q., Zhou, N., Zhang, Z., Du, M., 2020. Sensor. Actuator. B Chem. 306, 127608.
Li, Y.J., Ma, M.J., Zhu, J.J., 2012b. Anal. Chem. 84, 10492–10499.
Lin, Y., Sun, Y., Dai, Y., Sun, W., Zhu, X., Liu, H., Han, R., Gao, D., Luo, C., Wang, X., 2020. Talanta 207, 120300.
Ling, P., Lei, J., Ju, H., 2015. Biosens. Bioelectron. 71, 373–379.
Liu, C.S., Li, J., Pang, H., 2020a. Coord. Chem. Rev. 410, 213222.
Liu, J., Lu, Y., 2003. J. Am. Chem. Soc. 125, 6642–6643.
Liu, P., Li, X., Greenspoon, S.A., Scherer, J.R., Mathies, R.A., 2011a. Lab Chip 11, 1041–1048.
Liu, Q., Wang, H., Han, P., Feng, X., 2019a. Analyst 144, 6025–6032.
Liu, X., Hu, M., Wang, M., Song, Y., Zhou, N., He, L., 2019b. Biosens. Bioelectron. 123, 59–68.
Liu, X.Y., Mwangi, M., Li, X.J., O'Brien, M., Whitesides, G.M., 2011b. Lab Chip 11, 2189–2196.
Liu, Y., Wang, H., Xiong, C., Yuan, Y., Chai, Y., Yuan, R., 2016. Biosens. Bioelectron. 81, 334–340.
Liu, Z.Y., Shen, C.L., Lou, Q., Zhao, W.B., Wei, J.Y., Liu, K.K., Zang, J.H., Dong, L., Shan, C.X., 2020b. J. Lumin. 221, 117111.
Llewellyn, P.L., Bourrelly, S., Serre, C., Vimont, A., Daturi, M., Hamon, L., De Weireld, G., Chang, J.S., Hong, D.Y., Hwang, Y.K., Jhung, S.H., Férey, G., 2008. Langmuir 24, 7245–7250.
Luan, Q., Gan, N., Cao, Y., Li, T., 2017. J. Agric. Food Chem. 65, 5731–5740.
Luan, Q., Xiong, X., Gan, N., Cao, Y., Li, T., Wu, D., Dong, Y., 2018. Talanta 187, 27–34.
Luo, Z., Sun, D., Tong, Y., Zhong, Y., Chen, Z., 2019. Microchim. Acta 186, 1–10.
Ma, D., Zheng, S.R., Fan, J., Cai, S.L., Dai, Z., Zou, X.Y., Teng, S.H., Zhang, W.G., 2020. New J. Chem. 44, 1684–1688.
Ma, M.N., Zhuo, Y., Yuan, R., Chai, Y.Q., 2015. Anal. Chem. 87, 11389–11397.
Mishra, G.K., Sharma, V., Mishra, R.K., 2018. Biosensors 8, 1–13.
Mohammad, M., Razmjou, A., Liang, K., Asadnia, M., Chen, V., 2019. ACS Appl. Mater. Interfaces 11, 1807–1820.
Morris, W., Briley, W.E., Auyeung, E., Cabezas, M.D., Mirkin, C.A., 2014. J. Am. Chem. Soc. 136, 7261–7264.
Munzar, J.D., Ng, A., Juncker, D., 2019. Chem. Soc. Rev. 48, 1390–1419.
Nath, N., Chilkoti, A., 2002. Anal. Chem. 74, 504–509.
Neema, P.M., Tomy, A.M., Cyriac, J., 2020. Trac. Trends Anal. Chem. 124, 115797.
Ni, S., Zhuo, Z., Pan, Y., Yu, Y., Li, F., Liu, J., Wang, L., Wu, X., Li, D., Wan, Y., Zhang, L., Yang, Z., Zhang, B., Lu, A., Zhang, G., 2020. ACS Appl. Mater. Interfaces. https://doi.org/10.1021/acsami.0c05750.
Pardo-Yissar, V., Katz, E., Wasserman, J., Willner, I., 2003. J. Am. Chem. Soc. 125, 622–623.
Park, K.S., Ni, Z., Côté, A.P., Choi, J.Y., Huang, R., Uribe-Romo, F.J., Chae, H.K., O'Keeffe, M., Yaghi, O.M., 2006. Proc. Natl. Acad. Sci. U.S.A. 103, 10186–10191.
Paseta, L., Seoane, B., Julve, D., Sebastián, V., Téllez, C., Coronas, J., 2013. ACS Appl. Mater. Interfaces 5, 9405–9410.
Pham, T., Forrest, K.A., Franz, D.M., Space, B., 2017. CrystEngComm 19, 4646–4665.
Prasad, K.S., Cao, X., Gao, N., Jin, Q., Sanjay, S.T., Henao-Pabon, G., Li, X.J., 2020a. Sensor. Actuator. B Chem. 305, 127516.
Prasad, K.S., Abugalyon, Y., Li, C., Xu, F., Li, X., 2020b. 145, 5113-5117.
Qiao, X., Xia, F., Tian, D., Chen, P., Liu, J., Gu, J., Zhou, C., 2019. Anal. Chim. Acta 1050, 51–59.
Qiu, W., Gao, F., Yano, N., Kataoka, Y., Handa, M., Yang, W., Tanaka, H., Wang, Q., 2020. Anal. Chem. 92, 11332–11340.
Ren, Q., Mou, J., Guo, Y., Wang, H., Cao, X., Zhang, F., Xia, J., Wang, Z., 2020. Biosens. Bioelectron. 166, 112448.
Safaei, M., Foroughi, M.M., Ebrahimpoor, N., Jahani, S., Omidi, A., Khatami, M., 2019. Trac. Trends Anal. Chem. 118, 401–425.
Sanjay, S.T., Dou, M., Fu, G., Xu, F., Li, X., 2016a. Curr. Pharmaceut. Biotechnol. 17, 772–787.
Sanjay, S.T., Dou, M., Sun, J., Li, X., 2016b. Sci. Rep. 6, 30474.
Sanjay, S.T., Fu, G., Dou, M., Xu, F., Liu, R., Qi, H., Li, X., 2015. Analyst 140, 7062–7081.
Sanjay, S.T., Li, M., Zhou, W., Li, X., Li, X., 2020. Microsyst. Nanoeng. 6, 28.
Sanjay, S.T., Zhou, W., Dou, M., Tavakoli, H., Ma, L., Xu, F., Li, X.J., 2018. Adv. Drug Deliv. Rev. 128, 3–28.
Shahrokhian, S., Ranjbar, S., 2019. ACS Sustain. Chem. Eng. 7, 12760–12769.
Shahrokhian, S., Ranjbar, S., 2018. Analyst 143, 3191–3201.
Shao, K., Wang, B., Nie, A., Ye, S., Ma, J., Li, Z., Lv, Z., Han, H., 2018. Biosens. Bioelectron. 118, 160–166.

Shen, W.J., Zhuo, Y., Chai, Y.Q., Yuan, R., 2016. Biosens. Bioelectron. 83, 287–292.
Shen, W.J., Zhuo, Y., Chai, Y.Q., Yuan, R., 2015. Anal. Chem. 87, 11345–11352.
Shen, F., Li, X., Li, P.C.H., 2014. Biomicrofluidics 8, 014109.
Shen, F., Li, Y., Liu, Z., Li, X., 2017. Microfluid. Nanofluidics 21, 66.
Simon-Yarza, T., Mielcarek, A., Couvreur, P., Serre, C., 2018. Adv. Mater. 30, 1–15.
Song, Y., Duan, F., Zhang, S., Tian, J.Y., Zhang, Z., Wang, Z.W., Liu, C., Sen, Xu, Du, M., 2017. W.M. J. Mater. Chem. 5, 19378–19389.
Su, F., Zhang, S., Ji, H., Zhao, H., Tian, J.Y., Liu, C. Sen, Zhang, Z., Fang, S., Zhu, X., Du, M., 2017. ACS Sens. 2, 998–1005.
Tan, B., Wang, D., Cai, Z., Quan, X., Zhao, H., 2020. Sensor. Actuator. B Chem. 303, 127230.
Tang, L., Wang, Y., Li, J., 2015. Chem. Soc. Rev. 44, 6954–6980.
Tavakoli, H., Zhou, W., Ma, L., Perez, S., Ibarra, A., Xu, F., Zhan, S., Li, X.J., 2019a. Trac. Trends Anal. Chem. 117, 13–26.
Tavakoli, H., Zhou, W., Ma, L., Guo, Q., Li, X., 2019b. Nanotechnology and Microfluidics, pp. 177–209.
Tian, K., Ma, Y., Liu, Y., Wang, M., Guo, C., He, L., Song, Y., Zhang, Z., Du, M., 2020. Sensor. Actuator. B Chem. 303, 127199.
Tolentino, M.Q., Hartmann, A.K., Loe, D.T., Rouge, J.L., 2020. J. Mater. Chem. B 8, 5627–5635.
Tu, W., Dong, Y., Lei, J., Ju, H., 2010. Anal. Chem. 82, 8711–8716.
Wang, F., Wu, X., Yuan, X., Liu, Z., Zhang, Y., Fu, L., Zhu, Y., Zhou, Q., Wu, Y., Huang, W., 2017a. Chem. Soc. Rev. 46, 6816–6854.
Wang, M., Hu, M., Li, Z., He, L., Song, Y., Jia, Q., 2019c. Biosens. Bioelectron. 142, 111536.
Wang, S., Li, Z., Duan, F., Hu, B., He, L., Wang, M., Zhou, N., Jia, Q., Zhang, Z., 2019d. Anal. Chim. Acta 1047, 150–162.
Wang, S., Chen, Y., Wang, Shuya, Li, P., Mirkin, C.A., Farha, O.K., 2019a. J. Am. Chem. Soc. 141, 2215–2219.
Wang, S., McGuirk, C.M., Ross, M.B., Wang, Shuya, Chen, P., Xing, H., Liu, Y., Mirkin, C. A., 2017b. J. Am. Chem. Soc. 139, 9827–9830.
Wang, X.Z., Mao, X.Y., Zhang, Z.Q., Guo, R., Zhang, Y.Y., Zhu, N.J., Wang, K., Sun, P.P., Huo, J.Z., Wang, X.R., Ding, B., 2020. Inorg. Chem. 59, 2910–2922.
Wang, Y., Cao, W., Wang, L., Zhuang, Q., Ni, Y., 2018a. Microchim. Acta 185, 1–9.
Wang, Y., Li, L., Yan, L., Gu, X., Dai, P., Liu, D., Bell, J.G., Zhao, G., Zhao, X., Thomas, K. M., 2018b. Chem. Mater. 30, 3048–3059.
Wang, Y., Zhang, Y., Sha, H., Xiong, X., Jia, N., 2019b. ACS Appl. Mater. Interfaces 11, 36299–36306.
Wei, X., Zhou, W., Sanjay, S.T., Zhang, J., Jin, Q., Xu, F., Dominguez, D.C., Li, X., 2018. Anal. Chem. 90, 9888–9896.
Wu, H., Li, M., Wang, Z., Yu, H., Han, J., Xie, G., Chen, S., 2019a. Anal. Chim. Acta 1049, 74–81.
Wu, J., Yu, C., Yu, Y., Chen, J., Zhang, C., Gao, R., Mu, X., Geng, Y., He, J., 2020b. Sensor. Actuator. B Chem. 305, 127280.
Wu, Q., Tan, R., Mi, X., Tu, Y., 2020a. Analyst 145, 2159–2167.
Wu, S., Li, C., Shi, H., Huang, Y., Li, G., 2018. Anal. Chem. 90, 9929–9935.
Wu, S., Xin, Z., Zhao, S., Sun, S., 2019b. Nano Res 12, 2736–2742.
Xie, B.P., Qiu, G.H., Sun, B., Yang, Z.F., Zhang, W.H., Chen, J.X., Jiang, Z.H., 2019. Inorg. Chem. Front. 6, 148–152.
Xie, S., Ye, J., Yuan, Y., Chai, Y., Yuan, R., 2015. Nanoscale 7, 18232–18238.
Xu, W., Zhou, X., Gao, J., Xue, S., Zhao, J., 2017. Electrochim. Acta 251, 25–31.
Xu, X., Wang, X., Hu, J., Gong, Y., Wang, L., Zhou, W., Li, X.J., Xu, F., 2019. Electrophoresis 40, 914–921.
Yaghi, O.M., Li, G.M., Li, H.L., 1995. Nature 378, 703–706.
Yang, Q., Hong, J., Wu, Y.X., Cao, Y., Wu, D., Hu, F., Gan, N., 2019. ACS Appl. Mater. Interfaces 11, 41506–41515.
Yang, Q., Zhou, L., Wu, Y.X., Zhang, K., Cao, Y., Zhou, Y., Wu, D., Hu, F., Gan, N., 2018. Anal. Chim. Acta 1020, 1–8.
Yang, X., Lv, J., Yang, Z., Yuan, R., Chai, Y., 2017a. Anal. Chem. 89, 11636–11640.
Yang, Y., Yang, Z., Lv, J., Yuan, R., Chai, Y., 2017b. Talanta 169, 44–49.
Zhang, H.T., Zhang, J.W., Huang, G., Du, Z.Y., Jiang, H.L., 2014. Chem. Commun. 50, 12069–12072.
Zhang, J., Wei, X., Zeng, R., Xu, F., Li, X., 2017b. Future Science OA 3, FSO187.
Zhang, Q., Wang, C.F., Lv, Y.K., 2018. Analyst 143, 4221–4229.
Zhang, T., Song, Y., Xing, Y., Gu, Y., Yan, X., Liu, H., Lu, N., Xu, H., Xu, Z., Zhang, Z., Yang, M., 2019b. Nanoscale 11, 20221–20227.
Zhang, X., Yan, T., Wu, T., Feng, Y., Sun, M., Yan, L., Du, B., Wei, Q., 2019a. Biosens. Bioelectron. 135, 88–94.
Zhang, Z., Ji, H., Song, Y., Zhang, S., Wang, M., Jia, C., Tian, J.Y., He, L., Zhang, X., Liu, C., 2017a. Biosens. Bioelectron. 94, 358–364.
Zhou, N., Ma, Y., Hu, B., He, L., Wang, S., Zhang, Z., Lu, S., 2019b. Biosens. Bioelectron. 127, 92–100.
Zhou, N., Su, F., Guo, C., He, L., Jia, Z., Wang, M., Jia, Q., Zhang, Z., Lu, S., 2019a. Biosens. Bioelectron. 123, 51–58.
Zhou, W., Feng, M., Valadez, A., Li, X., 2020a. Anal. Chem. 92, 7045–7053.
Zhou, W., Sun, J., Li, X., 2020b. Anal. Chem. 92, 14830–14837.
Zhou, X., Guo, S., Gao, J., Zhao, J., Xue, S., Xu, W., 2017. Biosens. Bioelectron. 98, 83–90.
Zhou, Y., Li, C., Li, X., Zhu, X., Ye, B., Xu, M., 2018. Anal. Methods 10, 4430–4437.
Zhou, Y., Mahapatra, C., Chen, H., Peng, X., Ramakrishna, S., Nanda, H.S., 2020c. Curr. Opin. Biomed. Eng. 13, 16–24.
Zhu, H., Yuan, J., Tan, X., Zhang, W., Fang, M., Wang, X., 2019. Environ. Sci. Nano 6, 261–272.
Zhu, Q.L., Xu, Q., 2014. Chem. Soc. Rev. 43, 5468–5512.
Zuo, P., Li, X., Dominguez, D.C., Ye, B.C., 2013. Lab Chip 13, 3921–3928.